Journal of Alloys and Compounds 1039 (2025) 182973

Contents lists available at ScienceDirect

Journal of Alloys and Compounds

journal homepage: www.elsevier.com/locate/jalcom

Thermodynamic assessment of the system La-W-O with focus on the core oxide system La_2O_3-WO_3

Elena Yazhenskikh [a,*], Mariya E. Ivanova [b,c], Dmitry Sergeev [a,d], Michael Müller [a]

[a] Institute of Energy Materials and Devices (IMD), Structure and Function of Materials (IMD-1), Forschungszentrum Jülich GmbH, Jülich 52425, Germany
[b] Institute of Energy Materials and Devices (IMD), Materials Synthesis and Processing (IMD-2), Forschungszentrum Jülich GmbH, Jülich 52425, Germany
[c] Trakia University, Stara Zagora 6000, Bulgaria
[d] NETZSCH-Gerätebau GmbH, Selb, D-95100, Germany

ARTICLE INFO

Keywords:
La_2O_3-WO_3 system
Lanthanum tungstate
Phase diagram
Phase equilibria
Thermodynamic modelling
CALPHAD
Associate species model
Ceramic proton conductors

ABSTRACT

The binary system La_2O_3-WO_3 was thermodynamically assessed using the available experimental information on phase equilibria and thermodynamic properties of binary lanthanum tungstates. The Gibbs energies of eight compounds $(La_2O_3)_m(WO_3)_n$ were for the first time generated based on thermal (Differential Thermal Analysis-DTA), calorimetrical and EMF (Electro-motive force) measurements from the literature. The melting temperature of the compound $La_6W_2O_{15}$ was determined by high-temperature dilatometry. The modified associate species model was successfully applied for description of the liquid phase. The solid solution based on the compound $La_{10}W_2O_{21}$ (called LaWO) with defective fluorite type structure shows promising conductive properties and can be applied as proton conductor in various electrochemical devices. Therefore, this phase was included in the dataset and modelled using a multi-sublattice model. The calculations on phase equilibria and thermodynamic properties are in good agreement with the available experimental data. The dataset obtained can be used for calculations of the thermodynamic stability of the relevant ceramic phases in order to predict the properties of the complex systems containing functional materials and environmental conditions (temperature, chemical compositions).

1. Introduction

In the light of the global energy transition, in which the focus is on technologies for decarbonization and sustainability of energy production, storage and utilization in e.g., mobility and industrial sectors, there is the need for high performance materials as key technological enablers. The definition of materials with operational efficiency is therefore the cornerstone for the advancement of innovative technologies and their deployment in a multitude of applications. (Co-) Electrolysers, fuel cells, membrane reactors, H_2 pumps and compressors based on proton conducting ceramic materials are technologies with relatively low technological readiness and highly promising prospects due to several important advantages over other competitive technologies [1]. There is a variety of material choices depending on their function in such electrochemical devices, e.g., solid electrolyte, electrode for H_2 generation or for water splitting etc., offering various ranges of target properties for each mentioned application [2].

In the context of chemical industry decarbonization, electrochemical or pressurized proton conducting ceramic reactors for synthesis of various chemicals need to be based on robust and well-performing material classes. In this context, an important family of ceramic materials with protonic and mixed protonic-electronic conductivity is the family of lanthanide tungstates (LaWO), denoted generally as Ln_6WO_{12} with Ln = La, Ce, Pr, Nd, Sm, Eu, Gd, Tb, Er, Tm, Yb, Lu and Y. Its crystal structure can be described as ordered defective fluorite or disordered pyrochlores with two vacant interstitials in the oxygen lattice $Ln_6WO_{12}Va_2$ [3]. This structure transforms along the lanthanide series from cubic or pseudo-cubic for lanthanum to praseodymium, to pseudo-tetragonal from neodymium to gadolinium, to rhombohedral for the smaller rare-earth cations from terbium to lutetium and for yttrium [4]. This material class has attracted significant attention in the last two decades since the pioneering work by Shimura et al. [5] revealed proton conductivity of $3–5{\cdot}10^{-3}$ S/cm for La_6WO_{12} (with the highest value measured for $La_{5.8}WO_{12}$). Proton conductivity of La_6WO_{12} dominates below 1073 K [6]. Apart from the protonic or mixed protonic-electronic conductivity at elevated temperatures [7,8], materials of this family

* Corresponding author.
E-mail address: e.yazhenskikh@fz-juelich.de (E. Yazhenskikh).

https://doi.org/10.1016/j.jallcom.2025.182973
Received 10 April 2025; Received in revised form 9 July 2025; Accepted 10 August 2025
Available online 13 August 2025

exhibit less resistive grain boundaries compared to state-of-the-art ceramic proton conductors such as $BaZr(Ce,Y)O_3$. Additionally, these are materials with superior mechanical and chemical stability compared to a number of other ceramic classes and this is an appealing feature to promote their application in devices operating under harsh conditions including presence of CO_2, CO, H_2S, HCN, COS, steam, etc. and moderate pressure gradients [9–11]. Furthermore, a few compatibility studies reveal that LaWO is chemically stable in contact with other functional materials for electrochemical devices, such as 8YSZ, 8YSZ--NiO, CGO, MgO, in the 873–1073 K operational range [12], as well as $La_{0.7}Sr_{0.3}MnO_{3-\delta}$, $La_{0.75}Sr_{0.25}Cr_{0.5}Mn_{0.5}O_{3-\delta}$ but it reacts with $Ba_{0.5}Sr_{0.5}Co_{0.8}Fe_{0.2}O_{3-\delta}$, according to Quarez et al. [13]. All this makes these materials suitable to develop and scale up various membrane reactor concepts, e.g. water gas shift reactors or other devices for catalytic processing of chemicals [14–18].

The compositional area of this LaWO phase covers the range from $La_{10}W_2O_{21}$ and La_6WO_{12} depending on temperature. La_6WO_{12} could be described as a face-centred cubic structure with an inherently deficient oxygen sublattice which can be filled by proton defects ($OH^{\bullet}$) in presence of water vapor. According to latest structural studies, the general formula $La_{28-x}W_{4+x}O_{54+1.5x}Va_{2-1.5x}$ (LAWO) where $x = 0.74–1.08$ is adopted as the representative one for this class of proton conductors [19, 20].

The properties of the system La_2O_3-WO_3 are therefore crucial for synthesis and application of these oxide materials. The knowledge about stability of lanthanum tungstate depending on temperature and partial pressure of oxygen can support the development and design of promising membrane materials. A reliable dataset containing the thermodynamic functions for all phases is helpful for calculations and predictions of various thermodynamic properties (phase equilibria, heat capacity, transition temperature, phase stability, etc.) by variation of chemical composition, temperature, and pressure. The quality of the database, its reliability and completeness, is a key issue of thermodynamic calculations.

In the last decades, a new oxide and salt database has been developed [21,22] including various oxides, e.g. [23,24], and sulphides [25]. The database containing the oxides of alkali (Li, K, Na), earth-alkali (Ca, Mg), transition metals (Co, Cr, Cu, Fe, Mn, Ni), Al, Si, Zn, P has been thermodynamically assessed using all available experimental data on phase equilibria and thermodynamic properties [22]. This database is relevant for the development and production of refractory materials as well as for metallurgical slag applications, glass processing, or ash/slag formation during coal/biomass combustion and gasification [26].

The CALPHAD method [27] is implied to develop the thermodynamic database using all available experimental information on thermodynamic properties, such as phase equilibria, crystal structure, etc. The Gibbs energy (G) as a temperature-dependent (for a stoichiometric compound) or temperature-composition dependent function (for a solution phase) is generated for all phases. The corresponding thermodynamic parameters are optimised in the framework of the suitable thermodynamic model for each phase in order to provide a good agreement between measured and calculated data. The obtained dataset is used for further calculations and predictions.

The aim of the present work is the generation of a thermodynamic dataset for the binary system La_2O_3-WO_3 including the stoichiometric compounds and the solid and liquid solutions. In the literature, the phase equilibria data in the system lanthanum oxide - tungsten (VI) oxide have been experimentally studied using various methods, namely Differential Thermal Analysis (DTA), X-ray diffraction (XRD), high temperature X-ray diffraction (HT XRD) and chemical analysis, e.g. [28–32]. In the present work, the most reliable and consistent literature data on binary compounds with various ratios La_2O_3:WO_3 were critically evaluated and selected to be used in optimisation of thermodynamic parameters. The temperature dependences of the Gibbs energies for stoichiometric compounds were modelled considering the available thermochemical data, which were obtained in the literature by calorimetry and Electro-motive Force (EMF) methods. The proton-conductive phase LaWO based on $La_{10}W_2O_{21}$ and La_6WO_{12} is modelled using the multi-sublattice model in order to predict the solubility area in agreement with the experimental data. The sub-lattice model is the most applicable model for the description of the solid solubility in the oxide system, because this approach can consider the crystallographic information. The Gibbs energy of the liquid phase was modelled using a non-ideal associate solution model proposed by Besmann and Spear [33]. This model has been successfully applied for the description of melts containing oxides, sulphides and salts [22]. Since this dataset will be integrated into the general oxide-sulphide database [22], it enables the prediction of the interactions between oxide materials and environment, including the gas phase, slag, and other solid phases. Therefore, the associate species model is kept for the description of the liquid phase in the present work. The binary sub-systems La-O, W-O and La-W are not a main subject of the present study, but these systems were considered to have a complete description of the system La-W-O.

In addition, a preliminary experiment was done to prove the melting point of the compound with the ratio La_2O_3:WO_3= 3:2 using the dilatometry method with the purpose to clarify the contradictory information concerning the melting temperature of lanthanum tungstate.

2. Literature survey (available experimental data)

2.1. Phase diagram

Phase equilibria data in the binary system lanthanum oxide and tungsten (VI) oxide have been experimentally studied using various experimental techniques, namely thermal analysis, high temperature X-ray diffraction (HT XRD) or conventional XRD, chemical analysis.

The existence of several lanthanum tungstates with the compositional ratio La_2O_3:WO_3= 1:3, 11:9, 1:1, 3:2 and 3:1 was established by Tyushevskaya et al. [28]. A series of mixtures with mole fraction of La_2O_3 in steps of 0.05 was prepared using the conventional mixed-oxide route, the sintering was performed stepwise in the temperature range 1073–1973 K depending on the chemical composition in order to avoid possible melting. The structure of phases was identified by X-ray diffraction on powders. Furthermore, the solid-liquid equilibria in this system were presented in the concentration range from 0 to 0.80 mol fraction of La_2O_3 [29–32,34]. The first phase diagram up to appr. 0.33 mol fraction of La_2O_3 was proposed by Rode et al. [29] based on the results of DTA, XRD, and densimetric analysis. Similar methods were applied by Ivanova et al. [30] who determined the liquidus line in the concentration range of 0–0.75 mol fraction of La_2O_3. All samples were annealed to be equilibrated at various temperatures in the range of 1173–1673 K. The phase relationships were determined using thermal (DTA up to 1573 K, visual-polythermal curves coupled with microscopy in the range of 1273–2473 K) and structure methods (XRD). The solid solubilities on the basis of the compounds 1:1, 3:2 and 3:1 were proposed.

Casteels et al. [34] studied the thermodynamic stability and structure of the phases in the concentration range 0.75–1 mol fraction of La_2O_3, where the compounds 3:1 and 5:2 were identified. The vapour pressure measurements were performed using the KEMS method (Knudsen Effusion Mass Spectrometry) in the temperature range of 1800–2300 K. The residues of the effusion cell after measurements were examined by XRD.

The study of structure and phase equilibria was undertaken for rare earth tungstates by Yoshimura et al. [35]. High temperature X-ray diffraction (HT XRD) in combination with thermal analysis allowed to modify the phase diagram, in particular at high concentration of La_2O_3 and at high temperatures [31]. The solid solubility based on the crystallographic modifications of lanthanum oxides was proposed. Besides the conventional synthesis method, solid-state reaction, Yoshimura [36] used co-fusion and long annealing afterwards (7–10 days) to ensure their

homogeneity of the compounds obtained. The new compound with the composition La_2O_3:WO_3= 7:8 was introduced by Yoshimura et al. [31, 35], although this composition was mentioned as an end-member of the solid solution in the concentration range of 0.467–0.5 mol fraction of La_2O_3 by Ivanova et al. [30].

The lanthanum tungsten bronzes La_xWO_3 (x = 0.1–0.2) were prepared by solid state reaction at P = 3•10^9 Pa and T = 1320–1620 K and structurally and thermally characterized by X-ray diffraction, electron microscopy, and thermal analyses [37,38]. Since these phases can be obtained at high pressure only, they were not considered in the present work.

The representative phase diagrams from the literature are shown in Fig. 1. The pictures are taken from the original literature, and temperature is shown in °C. The compositions of all binary compounds in the system La_2O_3-WO_3 are listed in Table 1. The compound with the La_2O_3:WO_3 ratio of 2:3 could be obtained in a NaCl melt, but not found in the La_2O_3-WO_3 system [39]. Therefore, this composition was excluded in the present work. The compound 11:9 was considered in [30,32] as part of the solid solution based on the compound 3:2. Since this solubility was not confirmed in other structural study, e.g. in [31], and no thermodynamic data is found, the compound 11:9 was not considered in the present work. The compounds 2:9 and 9:10 were replaced in accordance with the corresponding literature by 5:22 and 7:8, respectively. The detailed data on the individual compounds is presented in the next chapters.

Table 1
Binary compounds in the system La_2O_3-WO_3.

Chemical formula	ratio La_2O_3: WO_3	mole fraction		Structure / Space group*	Note
		WO_3	La_2O_3		
$La_4W_9O_{33}$	2:9	0.818	0.182	data not available	replaced by 5:22 in [31]
$La_{10}W_{22}O_{81}$	5:22	0.815	0.185	Pbcn [31,32]	white [40]
$La_2W_3O_{12}$	1:3	0.75	0.25	C2/c [41,42]	colourless [42]; LT
$La_2W_2O_9$	1:2	0.667	0.333	$P\bar{1}$ [43]	
$La_4W_3O_{15}$	2:3	0.6	0.4	$P4_2/nmc$ [39]	not considered
$La_{18}W_{10}O_{57}$	9:10	0.526	0.474	$P\bar{6}2c$ [44]	replaced by 7:8 in the present work
$La_{14}W_8O_{45}$	7:8	0.533	0.467	Orthorhombic [31,35]	
La_2WO_6	1:1	0.5	0.5	LT: $P2_12_12_1$ [45]	white [45]
$La_{22}W_9O_{60}$	11:9	0.45	0.55	HT: $P\bar{4}$ or $P\bar{4}m2$ [32]	not considered
$La_6W_2O_{15}$	3:2	0.4	0.6	orthorhombic $C222_1$; LT [46]; HT [47]	white [46,47]
$La_{10}W_2O_{21}$	5:2	0.286	0.714	$F\bar{4}3m$ [48], Fm3 [36]	white [48]
La_6WO_{12}	3:1	0.25	0.75	disordered pyrochlore [49]	white [49]

*LT and HT – low- and high-temperature modifications, correspondingly

2.2. Thermodynamic properties of stoichiometric compounds

In the literature, the high temperature enthalpy increment was experimentally determined for the following lanthanum tungstates: $La_{10}W_2O_{21}$, $La_6W_2O_{15}$, the low temperature modification of La_2WO_6 [50], $La_{14}W_8O_{45}$, $La_2W_2O_9$, $La_2W_3O_{12}$ and $La_{10}W_{22}O_{81}$ [51]. In both studies, the measurements were carried out in a massive calorimeter with an isothermal shell (298 ± 0.01 K) in air in the temperature range 298–1500 K. The compounds were prepared by solid state reaction from oxides with long annealing at 1373–1673 K. The composition of the samples obtained was controlled by chemical analysis and X-ray study after preparation and during the calorimetric measurements. The heat capacity of the corresponding binary compounds was determined based on the measured values of the enthalpy. The temperature dependences of the heat content and the heat capacity were reported for the corresponding temperature intervals.

Chentzov et al. [52] studied the formation of La_6WO_{12} (3:1) using the electromotive force (EMF) method in a cell with Pt electrodes and ThO_2 doped with La_2O_3 as a solid electrolyte. Wustite was applied as a reference electrode. The measurements were carried out in vacuum (appr. 1.3–6.6•10^{-8} atm). The equation for the Gibbs energy of the reaction $3La_2O_3+W+3/2O_2 \rightarrow La_6WO_{12}$ was obtained in the temperature

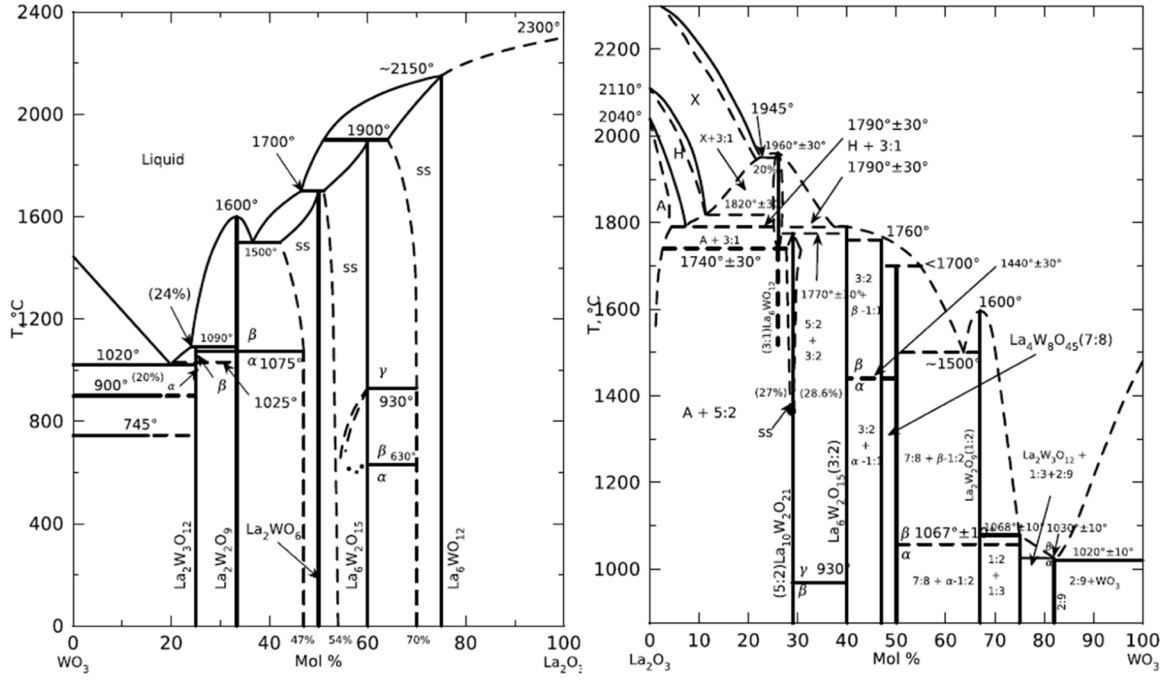

Fig. 1. Phase equilibria in the system La_2O_3-WO_3 according to the literature (left: Ivanova et al. [30]; right: Yoshimura and Rouanet [31]. The pictures are taken from the original literature, and temperature is shown in °C.

range 1200–1450 K. Based on these data, the formation enthalpies from oxides and elements were estimated for the compound 3:1. The standard formation enthalpy and standard entropy of La_6WO_{12} were derived. The further work of the same group [53,54] deals with a thermodynamic study of the interaction between the refractory oxides R_2O_3 where R stands for Al, Sc, Y, La, Nd, Dy, Gd with tungsten resulting in the formation of refractory tungstates. Levitskii et al. [53,54] reported the free energy and enthalpy of the formation reaction from La_2O_3+W+ $3/2O_2$ and from the oxides for the compound 3:1. The measured values [52,53] are in good agreement with each other.

The similar electrochemical cell was used in the works of Chanturishvili et al. [55,56] with the oxygen solid electrolytes based on ThO_2 doped with La_2O_3 or CaO. The stability of the phases was controlled during the measurements by XRD. The measured EMF of the corresponding reactions allowed the estimation of the formation Gibbs energy from lanthanum oxide, tungsten and oxygen. Further, the Gibbs energy for the formation reaction from elements or from the basic oxides (La_2O_3 and WO_3) was also estimated for the compounds $La_{10}W_{22}O_{81}$, $La_6W_2O_{15}$, La_2WO_6 (LT) [55] and $La_{14}W_8O_{45}$, $La_2W_2O_9$, $La_2W_3O_{12}$, and $La_{10}W_{22}O_{81}$ [56].

The Gibbs energy of formation of several lanthanum tungstates was determined by Raghavan [57] using the EMF method with LaOF as a solid electrolyte. The obtained values were not consistent with similar data from other literature sources: the Gibbs energy data were about 2.5 times less than those reported in [55,56,58] and thus not considered in the present work.

The thermodynamic data on the tungstates of the rare earth elements including the calorimetric measurements, the temperature dependencies of the Gibbs energies and the EMF values are collected in the handbook of Gwelesiani et al. [58], in which the standard thermodynamic functions, $\Delta_f H^\circ_{298}$ and S°_{298}, of these compounds were derived using the available heat capacity and the Gibbs energy data of formation from the basic oxides. Moreover, Nadiradze [59] estimated the standard entropy of tungstates of rare-earth elements ($REWO_x$) using the available experimental information. A similar method was used to determine the formation enthalpies of $REWO_x$ from the basic oxides [60]. All these estimated data are considered when determining the thermodynamic properties of LaWOx in the present work.

2.3. Structure of the LaWO phase

In the 1970s, two phase diagrams for the phase formation in the system La_2O_3 - WO_3 were published independently from each other [30,31]. They show, however, a significant mismatch in that part concerning the compounds with practically relevant La/W-ratios. Both suggest formation of $La_6W_2O_{15}$ and segregations of La_2O_3. Between these two compounds, Ivanova et al. [30] assumed the La_6WO_{12} phase to be present from room temperature to ~2423 K, while Yoshimura et al. [31] assumed a $La_{10}W_2O_{21}$ phase up to ~2063 K and assume La_6WO_{12} as a high-temperature phase from ~2013 K onwards. This means that Ivanova et al. [30] considers a La/W-ratio of 6 (denoted as LWO6) which corresponds to 0.75 mol fraction of La_2O_3, while Yoshimura *et al.* a La/W ratio of 5 (LWO5 or 0.714 mol fraction of La_2O_3). This discrepancy is also reflected in different publications. While most authors speak of a phase La_6WO_{12}, some call it $La_{10}W_2O_{21}$ [57,61]. However, it turned out that both assumptions cannot be true. Single-phase lanthanum tungstate can only be synthesized in the intermediate compositional range. According to Magrasó et al. [62,63], there is a single-phase range of La/W = 5.4–5.7 for a temperature treatment at 1773 K in air, while in Seeger et al. [64] this range is even narrower, La/W = 5.3 – 5.5 at 1773 K [64]. In any case, this stability window is processing method dependent and also temperature dependent and it shifts to smaller lanthanum contents with decreasing temperature. Such shifts are associated with the amount of oxygen vacancies generated in the structure: at higher temperature, structures contain larger amount of vacancies, therefore, the pristine material can dissolve more La. A similar trend was also observed in the case of Mo and Re substituted compositions [65,66], which are however beyond the scope of the present paper. The minimum temperature treatment to obtain single-phase pristine material is 1823 K for a La/W ratio of 5.8, 1673 K for La/W = 5.5 and 1373 K for La/W = 5.3 [62]. All this also leads to a revision of the crystal structure [19,20,65], initially proposed by Diot et al. [3]. For the lanthanum tungstate LWO5.6, the unit formula unit of $La_{6.63}W_{1.17}O_{13.43}$ was proposed and the crystal structure was presented as face-centred cubic with the space group $F\bar{4}3m$and lattice parameter being from 11.173 Å to 11.188 Å. The concentration of oxygen vacancies in the material is thus 11.2 per unit cell, corresponding to approximately three sites per formula unit. After further refinement of the crystal structure, the unit cell was formulated as $La_{28-x}W_{4+x}O_{54+\frac{3}{2}x}v_{2-\frac{3}{2}x}$ [20,67]. The regular structure thus corresponds to a La/W ratio of 28:4 = 7.0, being similar to that of $Y_7ReO_{14-\delta}$ [68]. The cations in the structure are ordered, with the tungsten occupying Wykoff site 4a and the lanthanum located on sites 4b and 24d. The charges are balanced in this case and the structure contains two intrinsic oxygen vacancies per unit cell. However, this regular structure is not stable due to the high number of oxygen vacancies. By substituting tungsten onto the La2 site, the crystal structure can be stabilized so that single-phase samples can be synthesized at room temperature. Assuming that tungsten exists in the structure as W^{6+} - a triple positively charged donor – one W donor will require 1.5 oxygen vacancies to balance the charge. For x = 1, i.e., LWO5.4, exactly one tungsten ion per unit cell is substituted onto a lanthanum site, consuming 1.5 oxygen vacancies and leaving 0.5 oxygen vacancies per unit cell. This results in the unit cell $La_{27}W_5O_{55.5}$. The crystal structure is stable when x in $La_{28-x}W_{4+x}O_{54+\frac{3}{2}x}v_{2-\frac{3}{2}x}$ is in the range of x = 0.74–1.08 and with a La/W ratio is in the range of 5.7–5.3 [20].

3. Dilatometry

There are two contradictory sets of experimental data in the literature that report different melting behaviour in the La_2O_3-rich concentration range. Ivanova et al. [30] proposed decomposition of 3:2 at 2173 K to the liquid phase and 3:1 based on the visual thermal curve, whereas Yoshimura and Rouanet [31] and Yanovskii and Voronkova [32] found congruent melting at 2063 K using HT XRD. In the present work, the melting temperature of $La_6W_2O_{15}$ was measured on sintered samples prepared from in-house-synthesised powder, using high temperature dilatometry (DIL402E, NETZSCH, Germany) with a graphite furnace under helium atmosphere. The samples for graphite holder were pre-sintered firstly in the dilatometer at 1723 K with a heating rate of 5 K/min and fast cooling with 30 K/min to get a stable form of the pellet. A green pellet was used for iridium holder, and the sintering takes place during the experiment. The dilatometric measurements were carried out with a heating rate of 5 K/min up to 2200 K. The temperature was validated with the melting of pure platinum. Three crucibles (supports) materials (tungsten, graphite and iridium) have been tested to find good compatibility with the sample.

As previously reported [46], $La_6W_2O_{15}$ powder was synthesized via a solid-state reaction using La_2O_3 (99.999 %, Sigma–Aldrich, CAS 1312–81–8) and WO_3 (99.9 %, Fluka) as starting materials. Prior to weighing, La_2O_3 was dried and decarbonated at 1000 °C for several hours. Stoichiometric amounts of the oxides were then weighed, mixed, milled in ethanol and finally dried to complete ethanol evaporation. The synthesis was conducted in a closed platinum crucible at 1000 °C for 12 h, with heating and cooling rates of 3 K/min. The resulting product was subsequently used for structural characterization, verification of chemical composition, stability assessment, and chemical compatibility studies (results reported elsewhere [46]). The stoichiometry of the synthesized $La_6W_2O_{15}$ powder was verified using inductively coupled plasma–optical emission spectrometry (ICP–OES). No deviations from the nominal chemical composition were detected. No secondary phases were identified by XRD analysis at room temperature, confirming the

phase purity of the synthesized $La_6W_2O_{15}$. The combination of earlier collected data from high-temperature X-ray diffraction and the dilatometry carried out in the present study provides a comprehensive view of the thermal evolution of $La_6W_2O_{15}$, supporting the understanding that melting occurs from a structurally stable, single-phase material, without detectable decomposition or phase separation.

4. Phases and thermodynamic models

The present database contains a liquid phase (called "Liquid"), one solid solution phase based on $La_{10}W_2O_{21}$ and La_6WO_{12} (LaWO phase) and eight solid stoichiometric compounds. The thermodynamic data of all phases in the system La_2O_3-WO_3 are summarised in Tables 2–8. The binary sub-systems La-O, W-O and La-W are not a subject of the present study; however, these sub-systems were adopted from other assessments with small modifications. Their description is collected in Chapter 6.2.

4.1. Stoichiometric compounds

The Gibbs energy function, G(T), of pure compounds is defined in terms of their enthalpy, H(T) and entropy, S(T), which in turn are functions of the heat capacity, Cp, and the respective absolute entities $\Delta_f H^{\circ}_{298}$ and S°_{298}, as follows:

$$G(T) = H(T) - T \bullet S(T); H(T) = \Delta_f H^0_{298} + \int_{298}^{T} C_p dT; S(T) = S^0_{298} + \int_{298}^{T} \frac{C_p}{T} dT$$

The Gibbs energy of tungsten (VI) oxide was adopted from the SGPS database [69] including the solid-solid transition and melting at 1050 K and 1745 K, respectively. These data are identical to those summarised by Chase et al. [70]. The data on lanthanum oxide were taken from the assessment performed by Grundy et al. [71]. Thermodynamic information on elements and oxides is collected in Table 2. Thermodynamic data (standard enthalpy of formation and standard entropy, $\Delta_f H^{\circ}_{298}$, S°_{298}, and $C_p(T)$ for stoichiometric lanthanum tungstates are generated in the present work and introduced in Chapter 6.3 in details (Tables 5–7). Thermodynamic properties including the data on the phase transitions are summarised below in the corresponding tables and figures.

4.2. Liquid phase

The Gibbs energy of the liquid phase in the system is represented by the modified non-ideal associate species model [33]. The oxides of La and W and one associate species ($La_2W_2O_9$) are considered as solution components. To provide equal weighting of each associate species with regard to its entropic contribution in the ideal mixing term, each species contains a total of two non-oxygen atoms per mole in its formula according to the model used in [33]: La_2O_3, W_2O_6, $La_2W_2O_9/2$, W_2O_4. The interactions between solution components were introduced in order to fine tune the thermodynamic description. The interactions between the species La_2O_3, W_2O_6 and $La_2W_2O_9/2$ determine the solid-liquid equilibria in the core system La_2O_3-WO_3.

The molar Gibbs energy of the solution is presented by a three-term expression with contributions of the reference part, the ideal and the excess part considering binary interactions as follows:

$$G_m = \sum x_i {}^{\circ}G_i + RT\sum x_i \ln x_i + \sum\sum_{i<j} x_i x_j \sum_{\nu=0} L_{ij}^{(\nu)} (x_i - x_j)^{\nu}$$

where x_i is the mole fraction of phase constituent i (including the associate species), ${}^{\circ}G_i$ is the molar Gibbs energy of the pure phase constituent and $L_{ij}^{(\nu)}$ with $\nu = 0$, 1 are the interaction coefficients between components i and j, according to the Redlich-Kister polynomial. ${}^{\circ}G_i$ and $L_{ij}^{(\nu)}$ are temperature dependent in the same way according to equation:

$${}^{\circ}G_i, \quad L_{ij}^{(\nu)} = A + B{\cdot}T + C{\cdot}T{\cdot}\ln(T) + D{\cdot}T^2 + E{\cdot}T^{-1}$$

Thermodynamic data for the liquid components are summarized in Table 3. The data on the liquid oxides such as WO_3•2 and La_2O_3 have been adopted from the SGPS database [69] and the work of Grundy et al. [71], respectively. In addition to the end-member oxides, one binary species $La_2W_2O_9/2$(liq) was added to provide a reasonable description of the melting behaviour in phase diagram, since otherwise the solid-liquid equilibria in the concentration range of 0.1–0.4 mol fraction of La_2O_3 could not be described properly using the interactions between La_2O_3(liq) and WO_3(liq) only. The Gibbs energy of the species $La_2W_2O_9/2$(liq) was created considering the data of the corresponding solid phase in order to obtain a better agreement with the experimental data on the phase relations. The interactions between the end-member oxides and the component $La_2W_2O_9/2$(liq) were added to improve the liquidus lines in the system La_2O_3-WO_3. The Gibbs energy data for the

Table 2
Thermodynamic data on elements and oxides used in the present work.

Liquid component	$\Delta_f H^{\circ}_{298}$, (J/mol)	S°_{298}, (J/mol•K)	T range, K: heat capacity Cp(T), (J/mol•K)	Reference
A-La_2O_3 (LT) H-La_2O_3 (MT) X-La_2O_3 (HT)	-1795548 -1749548 -1689548	127.341 147.229 172.407	298–2586: 118 + 0.016•T-1240000/T^2 2586–3500: 200	Grundy et al. [71]
WO_3 (LT)	−842908.6	75.91	298–600: 44.496 + 0.1320797•T−300279.4/T^2−8.276329•10^{-5}•T^2 600–1050: 129.3333–0.04960927•T−5936845/T^2 + 2.788372•10^{-5}•T^2	SGPS [69]
WO_3 (HT)	−841423.3	77.324	1050–1745: 80.96751 + 0.01634015•T + 6826.698/T^2 + 1.379699•10^{-8}•T^2 1745–3000: 131.796	
W_7O_{19}	−5468069.6	478.975	298–500: −470.44144 + 3.457888•T + 16132445/T^2−0.002970184•T^2 500–900: 603.97421 + 0.10576951•T−17276203/T^2−2.9068074•10^{-5}•T^2 900–1400: 706.2097–0.063834365•T−30286137/T^2+ 5.2991071•10^{-5}•T^2 1400–3000: 582.2425 + 0.08786631•T−3820.5027/T^2−7.332017•10^{-10}•T^2	SGPS [69]
WO_2	−589963	50.528	298–1200: 62.44 + 0.0249822•T−1194190/T^2−8.06677•10^{-6}•T^2 1200–2100: −130.398 + 0.1705375•T + 76446990/T^2 −3.289363•10^{-5}•T^2 2100–3000: 48.807 + 0.0272751•T + 8838740/T^2 −1.83478•10^{-6}•T^2	SGPS [69]
La (LT)	0	56.902	298–550: 26.34 + 0.002590331•T	SGPS [69]
La (MT)	364.0	57.564	550–1134: 21.79186 + 0.00809035•T + 3.155188•10^{-6}•T^2	
La (HT)	3485.3	60.316	1134–1193: 39.5388 1193–4000: 34.3088	
W	0	32.618	298–3695: 24.1 + 0.003872•T−89000/T^2−1.242•10^{-6}•T^2 + 6.396•10^{-10}•T^3 3695–6000: 54	SGPS [69]
O_2 (gas)	0	205.0376	298–900: 22.25862 + 0.02047734•T + 153499.1/T^2−8.039682•10^{-6}•T^2 900–3700: 33.55726 + 0.002469797•T −1079772/T^2−8–1.00166•10^{-7}•T^2	SGPS [69]

Table 3
Thermodynamic data on the liquid components.

Liquid component	$\Delta_f H^\circ_{298}$, (J/mol)	S°_{298}, (J/mol•K)	T range, K: heat capacity Cp(T), (J/mol•K)	Reference
La_2O_3 (liquid)	−1612978.3	202.016	298–2586: 118 + 0.016•T−1240000/T^2 2586–3500: 200	Grundy et al. [71]
WO_3 (liquid)	−767994.1	119.404	298–600: 44.496 + 0.1320797•T−300279.4/T^2−8.276329•10^{-5}•T^2 600–1050: 129.3333–0.04960927•T−5936845/T^2 + 2.788372•10^{-5}•T^2 1050–1745: 80.96751 + 0.01634015•T + 6826.698/T^2 + 1.379699•10^{-8}•T^2 1745–3000: 131.796	SGPS [69]
$La_2W_2O_9$ (liquid)	−3672456.33	317.21	298–1353: 325.5152 + 0.0050208•T−6301104/T^2 1353–1873: 355.05424	This work
WO_2 (liquid)	−506534	88.398	298–1200: 62.44 + 0.0249822•T−1194190/T^2−8.06677•10^{-6}•T^2 1200–2100: −130.398 + 0.1705375•T + 76446990/T^2 −3.289363•10^{-5}•T^2 2100–3000: 48.807 + 0.0272751•T + 8838740/T^2 −1.83478•10^{-6}•T^2	This work
La (liquid)	9681.80	65.51	298–550: 26.34 + 0.002590331•T 550–1134: 21.79186 + 0.00809035•T + 3.155188•10^{-6}•T^2 1134–1193: 39.5388 1193–4000: 34.3088	SGPS [69]
W (liquid)	52313.7	46.776	298–3695: 24.1 + 0.003872•T−89000/T^2−1.242•10^{-6}•T^2 + 6.396•10^{-10}•T^3 3695–6000: 54	SGPS [69]
O (liquid)	−2648.90	71.1335	298–1100: 11.294148 + 0.0097948•T + 71500.116/T^2 −3.70591794•10^{-6}•T^2 1100–3500: 16.807743 + 0.00118136002•T−510204.08/T^2 −3.4903191•10^{-8}•T^2 3500–6000: 12.326196 + 0.00261918•T + 14469647.2/T^2−1.79689014•10^{-7}•T^2	SGTE [72]

Table 4
Thermodynamic descriptions of the liquid and solid solution phases.

Gibbs energy data, J/mol	Reference
Liquid phase: (La_2O_3, W_2O_6, $La_2W_2O_9$/2, W_2O_4, W, O)	
$^\circ G_{La_2O_3} = {}^\circ G_{La_2O_3(liquid)}$	Grundy et al. [71]
$^\circ G_{W_2O_6} = 2 \bullet {}^\circ G_{WO_3(liquid)}$	SGPS
$^\circ G_{La_2W_2O_9/2} = 0.5 \bullet {}^\circ G_{La_2W_2O_9(liquid)} - 5687 + 3.5 \bullet T$	This work
$^\circ G_{W_2O_4} = 2 \bullet {}^\circ G_{WO_2(liquid)}$	This work
$^\circ G_{La} = {}^\circ G_{La(liquid)}$	SGPS
$^\circ G_{W} = {}^\circ G_{W(liquid)}$	SGPS
$^\circ G_{O} = {}^\circ G_{O(liquid)}$	SGPS
$^\circ L^{Liq}_{La_2O_3,La_2W_2O_9/2} = -119000, {}^1L^{Liq}_{La_2O_3,\ La_2W_2O_9/2} = -7500$	This work
$^\circ L^{Liq}_{W_2O_6,La_2W_2O_9/2} = -62000, {}^1L^{Liq}_{W_2O_6,\ La_2W_2O_9/2} = -16500$	This work
$^\circ L^{Liq}_{W_2O_6,W} = -53300$	This work
$^\circ L^{Liq}_{W,W_2O_4} = 108420 - 60 \bullet T$	This work
$^\circ L^{Liq}_{La_2O_3,La} = -93575 + 25 \bullet T$	This work
$^\circ L^{Liq}_{W,La} = 137856 - 1.41 \bullet T, L1^{Liq}_{W,La} = 1722$	This work
LaWO: $La^{3+}_{40}\ W^{6+}_6\ (La^{3+}, W^{6+})_2(O^{2-})_{81}(O^{2-}, Va)_3$ End-members: LaO=$La_{40}W_6La_2O_{81}O_3$ WO=$La_{40}W_6W_2O_{81}O_3$ LaVa=$La_{40}W_6La_2O_{81}Va_3$ WVa=$La_{40}W_6W_2O_{81}Va_3$	
$^\circ G_{LaO} = {}^\circ G_{WVa} = 3 \bullet {}^\circ G_{La_6WO_{12}} + 2 \bullet {}^\circ G_{La_{10}W_2O_{21}} + 1.5 \bullet {}^\circ G_{La_2O_3(LT)} + 131950 - 45.875 \bullet T$	This work
$^\circ G_{WO} = 4 \bullet {}^\circ G_{La_{10}W_2O_{21}}$	This work
$^\circ G_{LaVa} = 6 \bullet {}^\circ G_{La_6WO_{12}} + 3 \bullet {}^\circ G_{La_2O_3(LT)} + 263900 - 91.75 \bullet T$	This work
$^\circ L^{LAWO}_{La^{3+},W^{6+}:O^{2-}} = -169000 + 51 \bullet T, L^{LAWO}_{La^{3+},W^{6+}:O^{2-}} = -26000 - 57.5 \bullet T$	This work
$^\circ L^{LAWO}_{La^{3+},W^{6+}:Va} = -169000 + 51 \bullet T, L^{LAWO}_{La^{3+},W^{6+}:O^{2-}} - 26000 - 57.5 \bullet T$	This work

liquid phase are listed in Table 4, including the interactions involving the metallic species.

4.3. Description of LaWO phase

The recent structural studies on lanthanum tungstates in the compositional range 0.70–0.75 mol fraction of La_2O_3 performed by Magraso et al. [20,63] and Erdal et al. [67] concluded that the phases reported as 5:2 and 3:1 should be a solubility area depending on the composition and temperature. The present model is simplified, and doesn't directly consider the partial pressure of oxygen, whereas the formation of oxygen vacancies is linked with the substitution of W on La sites. The chemical formula of this solution phase can be written as $La_{28-x}W_{4+x}O_{54+\delta}$, (δ=1.5x), or to indicate the vacancy state $La_{28-x}W_{4+x}O_{54+1.5x}Va_{2-1.5x}$, where x gives the amount of tungsten on lanthanum positions, and Va refers to a vacant site and can be occupied by oxygen. According to Erdal et al. [67], the perfect parent structure corresponds to x = 0 with the ratio La/W= 7 (at 0.778 mol fraction of La_2O_3). This stoichiometry has two vacant oxygen sites per unit cell. The hypothetical structure was predicted by DFT in VASP, but cannot be synthesised under usual conditions (atmospheric pressure). Decreasing the ratio La/W, a certain amount of W ions substitutes on La sites. As LaWO is an oxide with a high degree of basicity, the oxidation state of W is expected to remain + 6, that is supported by XPS analysis (X-ray Photoelectron Spectroscopy) presented in [67]. Then, it follows that W being on La site forms 3 + charged donors: $W^{\bullet\bullet\bullet}_{La}$. The stoichiometry with La/W= 5.4 (0.73 mol fraction of La_2O_3) corresponds to x = 1, and one unit cell can be written as $La_{27}W_5O_{55.5}$. In this case, there is one W occupying a La site per unit cell, and 1.5 of the 2 native vacant oxygen sites are filled in order to keep electroneutrality.

The Compound Energy Formalism (CEF) [73] with 5 sublattices was used to model this solid solubility between the compounds 5:2 and 3:1. According to the structural formula $La_{28-x}W_{4+x}O_{54+1.5x}Va_{2-1.5x}$, the solution can be written as follows, considering the replacement of La by W and the appearing oxygen vacancy as follows:

$$La^{3+}_{40}\ W^{6+}_6\ (La^{3+}, W^{6+})_2(O^{2-})_{81}(O^{2-}, Va)_3$$

In this case, the formula of the solution was deliberately re-calculated to avoid non-integer numbers. Four end-members are $La_{40}W_6La_2O_{81}O_3$, $La_{40}W_6W_2O_{81}O_3$, $La_{40}W_6La_2O_{81}Va_3$ and $La_{40}W_6W_2O_{81}Va_3$, those are denoted as LaO, WO, LaVa and WVa, respectively. The nature of the model is shown on the compositional triangle (Fig. 2) representing the upper part of the La-W-O triangle. The positions of the four solution components are indicated and the model covers the quadrangle formed by them. The solution appears on the line joining La_2O_3 and WO_3, namely between the compositions of the compounds 3:1 and 5:2. Two solution components, LaO and WVa are charged and added to the model to keep the electroneutrality conditions. WO is neutral and corresponds to the compound 5:2, while LaVa is also neutral and corresponds to the composition with the higher content of La_2O_3 and is expressed by a mixture of the compound 3:1 and La_2O_3. The Gibbs energies of charged end-members are determined using the reciprocal reaction WO+LaVa=LaO+WVa with ΔG= 0:

$$\Delta G = {}^\circ G_{LaO} + {}^\circ G_{WVa} - {}^\circ G_{WO} - {}^\circ G_{LaVa}$$

In this case, $^\circ G_{LaO}$ and $^\circ G_{Wva}$ are equal and defined as $^\circ G_{LaO} =$

Table 5
Thermodynamic of $(La_2O_3)_m(WO_3)_n$ compounds: standard formation enthalpy at 298 K.

Compound	La_2O_3: WO_3	$\Delta_f H^\circ_{298}$, (kJ/mol)	Method	Reference
$La_{10}W_{22}O_{81}$	5:22	−27512.3 ± 113.47	handbook	Gwelesiani [58]
		−29039.8	handbook*	Gwelesiani [58]
		−28882.476	**optimised**	**this work**
$La_2W_3O_{12}$	1:3	−4718.30 ± 20.92	estimated	Plyuschev [86, 89]
		−4539.64	handbook	Glushko [88]
		−4539.6	estimated	Chentsov [90]
		−4280.7 ± 17.45	handbook	Gwelesiani [58]
		−4620.64	handbook*	Gwelesiani [58]
		−4092580.7	ab-initio	aiMP [87]
		−4607563.16	**optimised**	**this work**
$La_2W_2O_9$	1:2	−3707.024	handbook	Glushko [88]
		−3707.0	estimated	Chentsov [90]
		−3479.4 ± 13.72	handbook	Gwelesiani [58]
		−3749.99	handbook*	Gwelesiani [58]
		−3397.86	ab-initio	aiMP [87]
		−3750957.38	**optimised**	**this work**
$La_{14}W_8O_{45}$	7:8	−19299.1 ± 56.5	handbook	Gwelesiani [58]
		−20736.87	handbook*	Gwelesiani [58]
		−20680432.9	**optimised**	**this work**
La_2WO_6	1:1	−2807.464	handbook	Glushko [88]
		−2807.5	estimated	Chentsov 1974 [90]
		−2814.2 ± 5.4	handbook	Gwelesiani [58]
		−2712.42	ab-initio	aiMP [87]
		−2816811.55	**optimised**	**this work**
$La_6W_2O_{15}$	3:2	−7129.5 ± 17.6	handbook	Gwelesiani [58]
		−7474.05	handbook*	Gwelesiani [58]
		−7465060.9	**optimised**	**this work**
$La_{10}W_2O_{21}$	5:2	−11012.3 ± 23.4	handbook	Gwelesiani [58]
		−11045725.7	**optimised**	**this work**
La_6WO_{12}	3:1	−6410.72 ± 27.61	derived from EMF	Chentsov [90]
		−6411.98 ± 11.296	handbook	Glushko [88]
		−6414.49	derived from EMF	Chentsov [52]
		−6454366.4	ab-initio	aiMP [87]
		−6410578.82	**optimised**	**this work**

* corrected in this work: re-calculated from sum of oxides + dH from oxides presented in [58]

$^\circ G_{WVa} = 1/2(^\circ G_{WO} + {}^\circ G_{LaVa})$.

The molar Gibbs energy of the phase is expressed by the following formula:

$$G_m = y^I_{La^{3+}} y^{II}_{O^{2-}} {}^\circ G_{LaO} + y^I_{W^{6+}} y^{II}_{O^{2-}} {}^\circ G_{WO} + y^I_{La^{3+}} y^{II}_{Va} {}^\circ G_{LaVa} + y^I_{W^{6+}} y^{II}_{Va} {}^\circ G_{WVa} + 2RT(y^I_{La^{3+}} \ln y^I_{La^{3+}} + y^I_{W^{6+}} \ln y^I_{W^{6+}}) + 3RT(y^{II}_{O^{2-}} \ln y^{II}_{O^{2-}} + y^{II}_{Va} \ln y^{II}_{Va}) + G^{ex}_m$$

The molar excess Gibbs energy is expressed according to

$$G^{ex}_m = y^I_{La^{3+}} \cdot y^I_{W^{6+}} \cdot \sum_{k=0}^{n} L^k_{(La^{3+}, W^{6+}:O^{2-})} (y^I_{La^{3+}} - y^I_{W^{6+}})^k + y^I_{La^{3+}} \cdot y^I_{W^{6+}} \cdot \sum_{k=0}^{n} L^k_{(La^{3+}, W^{6+}:Va)} (y^I_{La^{3+}} - y^I_{W^{6+}})^k$$

where La^{3+} and W^{6+} are the cations on the cation sublattice, while

Table 6
Thermodynamic of $(La_2O_3)_m(WO_3)_n$ compounds: standard entropy at 298 K.

Compound	La_2O_3: WO_3	S°_{298}, (J/mol•K)	Method	Reference
$La_{10}W_{22}O_{81}$	5:22	1990.87 ± 93.39	handbook	Gwelesiani [58]
		2453.9 ± 90.4	estimated	Nadiradze [59]
		2306.7	estimated	Neumann-Kopp rule
		2103.93	**optimised**	**this work**
$La_2W_3O_{12}$	1:3	434.99	estimated	Plyuschev [86, 89]
		343.008	handbook	Glushko [88]
		380.7	estimated	Chentsov 1974 [90]
		348.5 ± 13.68	handbook	Gwelesiani [58]
		363.6 ± 10	estimated	Nadiradze [59]
		355.071	estimated	Neumann-Kopp rule
		340.83	ab-initio	aiMP [87]
		340.09	**optimised**	**this work**
$La_2W_2O_9$	1:2	280.3	estimated	Chentsov [90]
		266.19 ± 10.59	handbook	Gwelesiani [58]
		255.224	handbook	Glushko [88]
		275.3 ± 7.5	estimated	Nadiradze [59]
		271.79	ab-initio	aiMP [87]
		279.16	estimated	Neumann-Kopp rule
		266.59	**optimised**	**this work**
$La_{14}W_8O_{45}$	7:8	1477.54 ± 40.12	handbook	Gwelesiani [58]
		1428.8 ± 87.9	estimated	Nadiradze [59]
		1498.67	estimated	Neumann-Kopp rule
		1491.89	**optimised**	**this work**
La_2WO_6	1:1	200.8	estimated	Chentsov [90]
		201.3 ± 5.0	handbook	Gwelesiani [58]
		192.464	handbook	Glushko [88]
		206.3 ± 5.4	estimated based on EMF and dCp= 0	Chanturishvili [55]
		193.3 ± 7.5	estimated	Nadiradze [59]
		201.71	ab-initio	aiMP [87]
		203.251	estimated	Neumann-Kopp rule
		198.575	**optimised**	**this work**
$La_6W_2O_{15}$	3:2	507.5 ± 4.2	estimated	Nadiradze [59]
		525.1 ± 11.3	estimated based on emf and dCp= 0	Chanturishvili [55]
		509.2 ± 11.3	handbook	Gwelesiani [58]
		533.84	estimated	Neumann-Kopp rule
		517.56	**optimised**	**this work**
$La_{10}W_2O_{21}$	5:2	764.0 ± 13.4	estimated based on emf and dCp= 0	Chanturishvili [55]
		768.6 ± 64.4	estimated	Nadiradze [59]
		828.4 ± 13.3	handbook	Gwelesiani [58]
		788.52	estimated	Neumann-Kopp rule
		811.60	**optimised**	**this work**
La_6WO_{12}	3:1	472.792 ± 8.79	derived from EMF	Chentsov [90]
		460.65	derived from EMF	Chentsov [52]
		471.955 ± 8.368	handbook	Glushko [88]
		454.76	ab-initio	aiMP [87]
		457.93	estimated	Neumann-Kopp rule
		472.86	**optimised**	**this work**

Table 7
Heat capacities and transition data of $(La_2O_3)_m(WO_3)_n$ compounds.

Compound	Cp(T) (temperature range, K)	Method	Reference
$La_{10}W_{22}O_{81}$	2551.44504 + 0.66718064•T - 60429512/T^2 (298–1303)	calorimetry	Chanturishvili [51]
$La_2W_3O_{12}$	LT, HT: 352.58568 + 0.1158968•T - 6581432/T^2 (298–1363*) dH_{tr}= 1.844 kJ at 1303 K	calorimetry	Chanturishvili [51]
$La_2W_2O_9$	LT: 325.5152 + 0.0050208•T - 6301104/T^2 (298–1362); dH_{tr}= 43.514 kJ at 1353 K HT: 355.05424 (1362–1873*)	calorimetry	Chanturishvili [51]
$La_{14}W_8O_{45}$	1293.81832 + 0.5255104•T - 18974440/T^2 (298–1947*)	calorimetry	Chanturishvili [51]
La_2WO_6	LT, HT: 215.56 + 0.02644288•T−4288600/T^2 (298–2033*) dH_{tr}= 0.447 kJ at 1713 K	calorimetry	Nadiradze [50]
$La_6W_2O_{15}$	LT: 511.20112 + 0.06669296•T−3836728/T^2 (298−903) dH_{tr}= 1.715 kJ at 903 K MT: 295.01384 + 0.41605696•T (903–1203) dH_{tr}= 6.40 kJ at 1203 K HT: 567.60144 + 0.0602496 •T (1203–2065*)	calorimetry	Nadiradze [50]
$La_{10}W_2O_{21}$	802.03096 + 0.08510256•T - 17158584/T^2 (298–2050*)	calorimetry	Nadiradze [50]
La_6WO_{12}	423.0632 + 0.09424107•T - 4200970.8/T^2 −1.566676•10^{-5} •T^2 (298–2400)	estimation	NK, this work

* extrapolated to the melting temperature

Table 8
Formation enthalpy of $(La_2O_3)_m(WO_3)_n$ from the end-member oxides, La_2O_3 and WO_3 at 298 K.

Compound	La_2O_3: WO_3	ΔH_{298}^{oxides} (kJ/mol)	Method	Reference
$La_{10}W_{22}O_{81}$	5:22	−1527.37 ± 85.02	handbook	Gwelesiani [58]
		−1348.1 ± 169.5	estimated	Nadiradze [60]
		−1507.67	**optimised**	**this work**
$La_2W_3O_{12}$	1:3	−298.24 ± 12.93	handbook	Gwelesiani [58]
		−252.7 ± 38.5	estimated	Nadiradze [60]
		−283.287	**optimised**	**this work**
$La_2W_2O_9$	1:2	−270.5 ± 10	handbook	Gwelesiani [58]
		−227.2 ± 41.4	estimated	Nadiradze [60]
		−269.59	**optimised**	**this work**
$La_{14}W_8O_{45}$	7:8	−1437.8 ± 35.6	handbook	Gwelesiani [58]
		−1262.7 ± 131.8	estimated	Nadiradze [60]
		−1368.31	**optimised**	**this work**
La_2WO_6	1:1	−177.5 ± 4.6	handbook	Gwelesiani [58]
		−178.7 ± 4.6	estimated based on emf and dCp= 0	Chanturishvili [55]
		−167.8 ± 10	estimated	Nadiradze [60]
		−178.35	**optimised**	**this work**
$La_6W_2O_{15}$	3:2	−407.2 ± 10.0	handbook	Gwelesiani [58]
		−367 ± 10.0	estimated based on emf and dCp= 0	Chanturishvili [55]
		−386.2 ± 16.7	estimated	Nadiradze [60]
		−392.60	**optimised**	**this work**
$La_{10}W_2O_{21}$	5:2	−358.1 ± 11.7	handbook	Gwelesiani [58]
		−364.0 ± 11.7	estimated based on emf and dCp= 0	Chanturishvili [55]
		−419.2 ± 64.4	estimated	Nadiradze [60]
		−382.16	**optimised**	**this work**
La_6WO_{12}	3:1	−183.26 ± 25.9	estimated from EMF	Chentsov [90]
		−192.0	estimated from EMF	Chentsov [52]
		−181.03	**optimised**	**this work**

oxygen and vacancies (Va) occupy the anion sublattice. The values of $L^k_{(La^{3+},W^{6+}:O^{2-})}$ and $L^k_{(La^{3+},W^{6+}:Va)}$ are the interaction parameter between the corresponding cations, while the anion sublattice is occupied by oxygen or vacancy, respectively.

The terms of the Gibbs energy for each constituent (Table 2) are composed from those Gibbs energies of the corresponding compounds, whose data were obtained in the present work (Chapter 6.3). It should be noted that the Gibbs energy of the solution component LaVa only was adjustable for the correct representation of the solubility range of the LaWO phase according to the experimental data on phase equilibria. Additionally, the interaction parameters L were also optimised for better representation of the experimental data (Table 4).

5. Assessment of thermodynamic data

In the present work, the Gibbs energies of eight compounds and two solution phases in the system La_2O_3-WO_3 were generated using the experimental data on phase equilibria and thermodynamic properties. The elemental sub-systems were firstly considered and tested in terms of the accuracy and correctness of the data adopted from the commercial datasets. The main focus of the present work is the thermodynamic assessment of the oxide system La_2O_3-WO_3. Primary, the heat capacity polynomials of the LaWOx compounds were defined using the calorimetric results published in the literature. In case of absence of measured Cp data (the compound 3:1, La_6WO_{12}), the heat capacity was modelled using the Neumann-Kopp approach from the heat capacities of the end-member oxides, La_2O_3 and WO_3. Then, the values of the standard formation enthalpies and standard entropies were adopted from the literature and optimised to provide a good agreement between the experimental and calculated phase equilibria data and the thermodynamic properties of the stoichiometric compounds. Secondly, the interactions in the liquid phase between the basic oxides, La_2O_3 and WO_3•2, and the component $La_2W_2O_9$/2(liq) were added to reproduce the correct melting behaviour of the lanthanum tungstates according to the experimental data. Next, the Gibbs energy data of the solution constituents in the phase LaWO were optimised to introduce the solid solubility range between the 5:2 and 3:1 compounds in accordance with the data of Magraso et al. [62].

All calculations were performed using FactSage 8.3 package [74]. The parameter optimisation was performed using OptiSage and Calphad Optimiser [75] in FactSage.

6. Results and discussion

The results of the critical evaluation and thermodynamic assessment

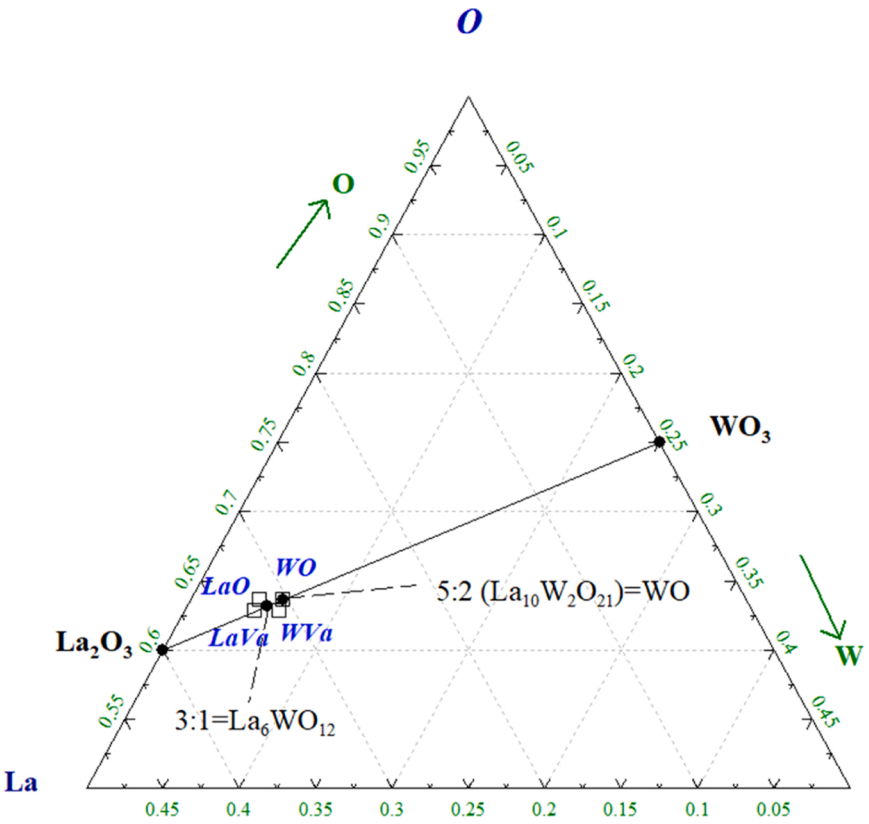

Fig. 2. The schema for the phase LaWO located on the line La_2O_3-WO_3 in the compositional triangle $La_{0.5}O_{0.5}$-O-$W_{0.5}O_{0.5}$.

of all phases (eight stoichiometric compounds, solid solution LaWO, liquid phase) and phase equilibria in the oxide system La_2O_3-WO_3 are presented in this chapter. Firstly, the preliminary experimental results validating the melting point of the compound $La_6W_2O_{15}$ using the dilatometry method are presented. Secondly, the elemental sub-systems La-O, W-O and La-W are considered. Finally, the thermodynamic description of the oxide system La_2O_3-WO_3 is presented considering the liquid and all solid phases. The data on the standard formation enthalpy, the standard entropy, the heat capacity, and the formation enthalpies from the basic oxides (La_2O_3 and WO_3) for the stoichiometric compounds $LaWO_x$ with various ratios of oxides are collected in Tables 5-8. The calculated phase equilibria data are compared with the experimental data and summarised in Table 9.

6.1. *Melting temperature of the compound $La_6W_2O_{15}$*

Regarding the HT dilatometric measurements of the melting temperature of the compound $La_6W_2O_{15}$, the choice of an appropriate crucible material was the main challenge. At the first attempt, the sample was found to react with tungsten, and no clear melting signal was seen on the DIL curve. In the case of a graphite crucible, two experiments were carried out. For the first experiment, the sample was aligned coaxially with the sample holder, where the contact area is relatively large. As a result of this experiment, the sample did not melt even when heated up to 2273 K (Supplementary, Fig. 3X). As shown on Fig. 3XX, the sample retained its shape after the experiment while simultaneously reacting with graphite. Therefore, in the next step, the sample was placed across the holder to reduce the contact area (Supplementary, Fig. 3XXX). In this case, the melting point of the sample (black line) at a temperature of 2113 K (raw data without temperature calibration) is clearly visible (Fig. 3). Considering the calibration with the melting temperature of platinum, the melting temperature of $La_6W_2O_{15}$ is 2158 K. To verify this result, an additional experiment was carried out with an iridium crucible (Fig. 3). As can be seen in Fig. 3, a significant change in the length of the sample is observed above 1273 K, which is due to the sintering of the sample. At a temperature of 2084 K (after calibration 2129 K), a decrease in the signal occurs, indicating that the melting temperature has been reached. In this case, however, this effect is not as pronounced as with a graphite crucible, as the sample was aligned coaxially with the sample holder and had high contact surface with the iridium. Therefore, we suggest to use the melting temperature obtained with the graphite sample holder 2158 ± 30 K based on these experimental results.

Based on the present dilatometry results, we cannot undoubtedly conclude which phase equilibria data are more reliable. The measured point of 2158 K may indicate congruent melting of 3:2 found by Yoshimura and Rouanet [31] as well as the decomposition of this phase reported by Ivanova [30]. In the latter case, the subsequent melting point cannot be measured due to the temperature limit of the dilatometer used. So, the data obtained can therefore be considered as preliminary information on the melting temperature of this compound along with other experimental data. However, further experimental study is necessary for clarification, but it is outside the scope of the present paper.

6.2. *Sub - systems La-O, W-O, La-W*

The system La-O was thermodynamically evaluated by Grundy et al. [71], the data on lanthanum oxide (solid and liquid) were taken from this assessment without modifications. In the present work, the phase names La_2O_3-LT, -MT and -HT are for the low-, medium- and high-temperature phases used instead of the conventional names of crystallographic modifications (A, H and X, respectively). The Gibbs energy of the liquid phase in the system is represented in the framework of the modified associate species model with the following components: La (liq), O (liq), La_2O_3 (liq). Thermodynamic data on La and O in the solid and liquid phases are adopted from the SGPS database [69]. The calculated phase diagram of the system La-O is shown in Supplementary,

Table 9
Invariant points in the binary La_2O_3-WO_3 system. The transition temperatures are given in K and in °C for clarity.

Reaction	Reaction type	Mole fraction La_2O_3	T, K (°C)	Reference
$La_{10}W_{22}O_{81}$ (s) + WO_3 (HT) ↔ Liq	eutectic	0.2	1293 (1020)	[29,30]
		< 0.182	1293 (1020)	[31,32]
		0.183	**1301 (1028)**	**this work**
$La_4W_9O_{33}$ (s)* ↔ Liq	melting	0.182	1303 (1030)	[31]
$La_{10}W_{22}O_{81}$ (s) ↔ Liq	melting	0.185	1303 (1030)	[32,99]
			1301 (1028)	**this work**
$La_2W_3O_{12}$ (LT) ↔ $La_2W_3O_{12}$ (HT)	solid-solid transition	0.25	1298 (1025)	[29,30]
			1170 (897)	DTA, single crystal [84]
			1308 ± 15 (1035)	DTA, [41]
			1303 (1030)	[31], XRD
			1285 (1012)	[31], DTA
			1303 (1030)	**this work**
$La_2W_3O_{12}$ (HT) ↔ Liq	melting	0.25	1363 (1090)	Rode [29]
			1338 ± 10 (1065)**	[41], DTA
			1413 (1140)**	[83], DTA
			1370 (1097)**	DTA, single crystal [84]
$La_2W_3O_{12}$ (HT) ↔ Liq + $La_2W_2O_9$ (HT)	incongruent melting	0.25	1363 (1090)	[30], DTA
			1341 (1068)	[31], TA
			1355 (1082)	**this work**
			1348 (1075)	DTA [29,30]
			1340 ± 10 (1067)	HT XRD [31,99]
$La_2W_2O_9$ (LT) ↔ $La_2W_2O_9$ (HT)	solid-solid transition	0.333	1362 ± 5 (1089)	Calorimetry [51]
			1350 (1077)	DTA [91]
			1353 (1080)	DTA [92]
			1353 (1080)	**this work**
$La_2W_2O_9$ (HT) ↔ Liq	melting	0.333	1823 (1550)	[29]
			1873 (1600)	[30,32]
			1870 (1597)	TA [31]
			1881 (1608)	**this work**
$La_2W_2O_9$ (HT) + $La_{14}W_8O_{45}$ ↔ Liq	eutectic	0.362	1773 (1500)	[30]
			1755 (1482)	**this work**
$La_{14}W_8O_{45}$ ↔ Liq + La_2WO_6	peritectic		1773 (congr.) (1500)	[30]
			below 1973 (1700)	[31]

Table 9 (*continued*)

Reaction	Reaction type	Mole fraction La_2O_3	T, K (°C)	Reference
		0.43	**1971 (1698)**	**this work**
La_2WO_6 (LT) ↔ La_2WO_6 (HT)	solid-solid transition	0.5	1683 (1410)	[35]
			1713 ± 30 (1440)	[31], TA, HT XRD
			1745 (1472)	[95], cool., DSC
			1765 (1492)	[95], heat., DSC
			1763 (1490)	[95], HT XRD
			1713 (1440)	**this work**
La_2WO_6 ↔ Liq	melting	0.5	1973 (1700)	[30,34]
			2033 (1760)	[31]
			1963 (1690)	[32]
			2034 (1761)	**this work**
$La_6W_2O_{15}$ (LT) ↔ $La_6W_2O_{15}$ (MT)	solid-solid transition	0.6	903 (630)	[28–30]
			892 (619)	DTA, on heat. [31]
			872 ± 5 (599)	[50]
			888 (615)	DTA, on heat. [47]
			903 (630)	**this work**
$La_6W_2O_{15}$ (MT) ↔ $La_6W_2O_{15}$ (HT)	solid-solid transition	0.6	1223 (950)	[29]
			1203 (930)	[30]
			1202 (929)	DTA, on heat. [31]
			1194 ± 5 (921)	[50]
			1217 (944)	DTA, on heat. [47]
			1203 (930)	**this work**
$La_6W_2O_{15}$ (HT) ↔ Liq	melting	0.6	2173 (inc.) (1900)	[30]
			2063 (1790)	[31,32]
			2158 (1885)	**this work, exp. (dilatometry)**
			2158 (1885)	**this work, calc.**
$La_6W_2O_{15}$ (HT) + LaWO ↔ Liq	eutectic	0.647	**2140 (1867)**	**this work**
La_2O_3 (HT) + Liq ↔ LAWO	peritectic	0.738	**2194 (1921)**	**this work**

* the compound 2:9 was replaced by the composition 5:22 (La_2O_3:WO_3) according to the reported thermodynamic data parameters of the formation.
**the melting behaviour in [41,83,84] was not specified (congruent melting or the point on the liquidus line)

Fig. S1. The solubilities of oxygen in La_2O_3 and La described by Grundy et al. [71] are omitted here.

The phase diagram of the system W-O was proposed by Wriedt [76]. The peritectic decomposition of tungsten oxide (IV) at 1803 K, congruent melting of tungsten oxide (VI) at 1747 K and formation of several intermediate WO_x in the concentration range 72–74 at% of O were postulated in the absence of reliable experimental information. In the present work, the liquid phase was tentatively modelled in the framework of the chosen model with the liquid species W, O and two tungsten oxides (IV, VI). All stoichiometric compounds (W, WO_2, WO_3,

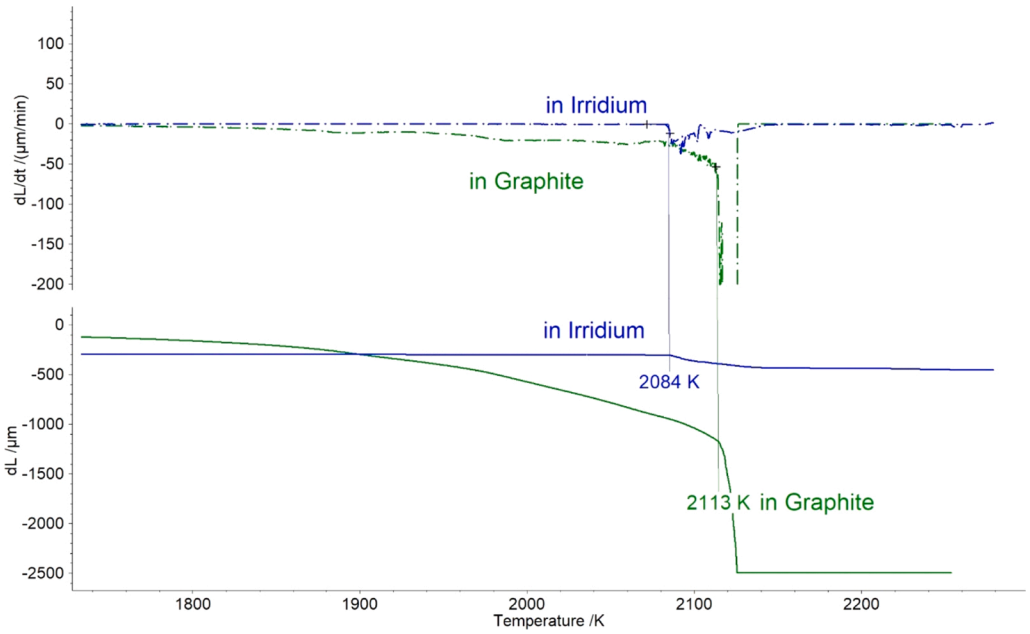

Fig. 3. Dilatometric signal (length change - dL with the temperature) and its differential (dL/dt) of the studied $La_6W_2O_{15}$ sample in the graphite and iridium crucibles for melting temperature determination.

W_7O_{19}) and the gas phase are adopted from the SGPS database. The calculated phase diagram is presented in Supplementary, Fig. S2. The melting behaviour of WO_2 and WO_3 are kept in accordance with Wriedt [76].

The solubility of W in liquid La was determined by Dennison et al. [77] from 1598 K to 2423 K and by Gaume-Mahn et al. [78] (up to 1473 K). The first data were considered as the more reliable ones and thus used to draw a partial phase diagram published by Predel [79]. Later, Okamoto [80] calculated the phase diagram based on the preliminary assessment of Krishnamurthy [81] who used the regular solution approximation and proposed the large miscibility gap at high temperature. In the present work, the interaction parameter between W (liq) and La(liq) (Table 4) was adjusted to reproduce the solubility in the La-rich concentration range (Fig. S3a). The calculated eutectic and

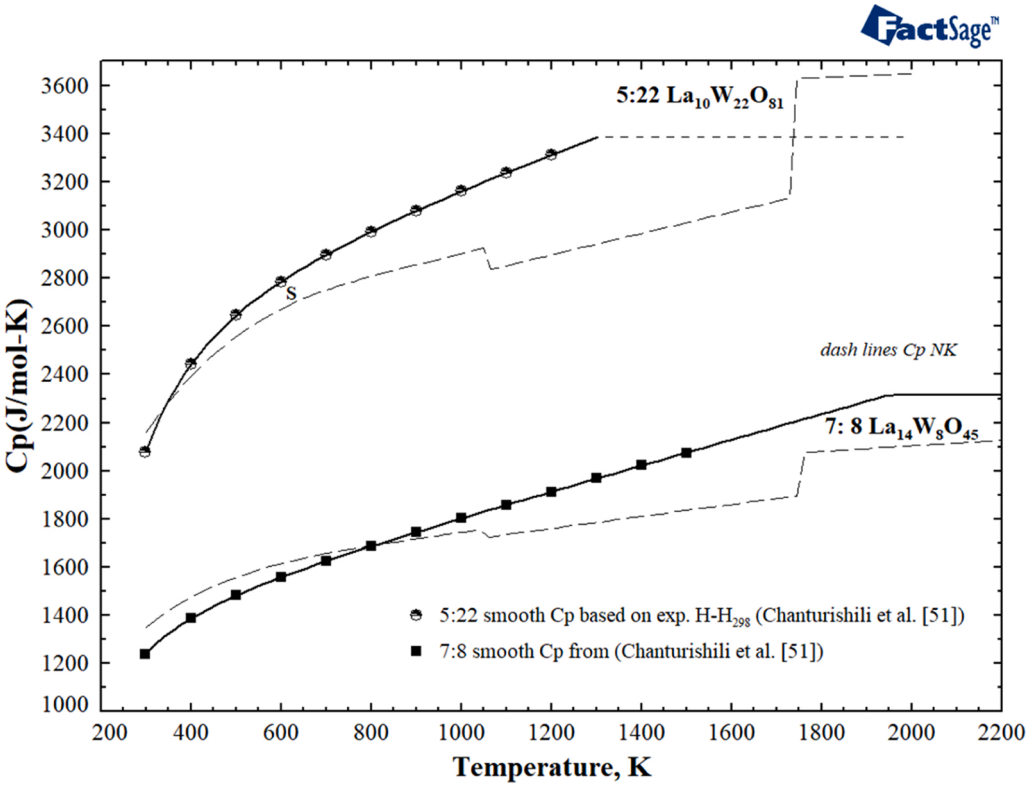

Fig. 4. Calculated heat capacity (solid line) of compounds 5:22 and 7:8 ($La_{10}W_{22}O_{81}$ and $La_{14}W_8O_{45}$) based on calorimetric data [51] in comparison with the Neumann-Kopp approach (dashed line).

monotectic temperatures are 1193 K and 3667 K, respectively (Fig. S3b) that is close to that proposed by Krishnamurthy [81] (1191 K) and Okamoto [80] (3667 K).

6.3. Thermodynamic modelling of stoichiometric compounds $(La_2O_3)_m(WO_3)_n$

6.3.1. Compound $La_{10}W_{22}O_{81}$ (La_2O_3:WO_3=5:22)

The compound $La_{10}W_{22}O_{81}$ was introduced by Yoshimura and Rouanet [31] to replace the previous mentioned composition 2:9 ($La_4W_9O_{33}$) that was found in the systems Re_2O_3-WO_3 for La-Nd in the earlier studies of Yoshimura et al. [82]. According to the studies of Yoshimura et al. [31,40] and to the later work of Yanovskii and Voronkova [32], this compound crystallises in an orthorhombic symmetry Pbcn and melts congruently at 1303 K.

In the present work, the heat capacity of the compound with highest content of WO_3 was modelled using the calorimetric data of Chanturishvili et al. [51], who derived the temperature dependency of the heat capacity from the enthalpy increment data. This equation was adopted in the present work without modifications and used for calculation of Cp up to the melting point (Table 7, Fig. 4). The experimental data on the enthalpy increment of $La_{10}W_{22}O_{81}$ [51] are compared with the calculated values in Fig. 5.

The Gibbs energy of the formation of 5:22 from the oxides (ΔG_f^{ox}) was estimated based on the EMF measurements [56] in the relative narrow temperature range 1134–1175 K and summarised in the handbook [58]. The calculated values of ΔG_f^{ox} related per mole of oxides are within the experimental error [56] (Fig. S4). Note that the obtained values are given per mole of crystalline oxide. The aforementioned reaction of formation can be written for any lanthanum tungstate as follows:

$$mLa_2O_3 + nWO_3 = (La_2O_3)_m(WO_3)_n$$

In case of a compound La_2O_3:WO_3=m:n, the presented Gibbs energy values (Fig. S4) are calculated from ΔG_f^{ox} divided by (m+n) for a better representation of various compositions.

The discrepancy between experimental and modelled values can be explained by the fact, that the optimisation of thermodynamic data of this compound was done after the compounds with high La_2O_3 content melting at higher temperatures. Thus, the phase diagram data were preferred to the Gibbs energy data by optimizing of 5:22. The optimised values of $\Delta_f H^\circ_{298}$, S°_{298}, Cp and $\Delta H^{ox}_{298,f}$ are compared with the available literature data in Tables 5–8.

6.3.2. Compound $La_2W_3O_{12}$ (La_2O_3:WO_3=1:3)

The synthesis and properties of the "middle" tungstate $La_2(WO_4)_3$ (1:3) were firstly studied by Plyuschev et al. [83]. The product of the interaction of the oxides is stable until 1323 K and has a monoclinic structure. The melting temperature of 1413 K was reported there without an explanation of the exact melting behaviour. This value differs from those published in other studies. Using DTA measurements Nassau et al. [41] and Brixner and Sleight [84] obtained the values of the melting temperature of 1338 K and 1370 K, respectively. The latest value is close to 1363 K published by Rode et al. [29] (congruent melting) and Ivanova et al. [30] (peritectic decomposition). The ambiguous character of the melting was explained by the fact that the peritectic composition (0.24 mol fraction of La_2O_3) is located very close to the composition of the compound (0.25) [30].

The authors [29–31,41] agreed on the temperature of polymorphic phase transition at 1298–1308 K, which is close to the temperature of the eutectic between 1:3 and WO_3 at 1293 K. The structural transformation of the single crystal of $La_2(WO_4)_3$ found by Brixner and Sleight [84] at 1170 K was not observed by calorimetric measurements up to 1238 K [51]. This structural transition was observed for several tungstates of the lanthanides $Ln_2(WO_4)_3$ with Ln=La, Ce, Pr, Nd, Sm, Eu in the temperature range 1243–1303 K, while the low-temperature

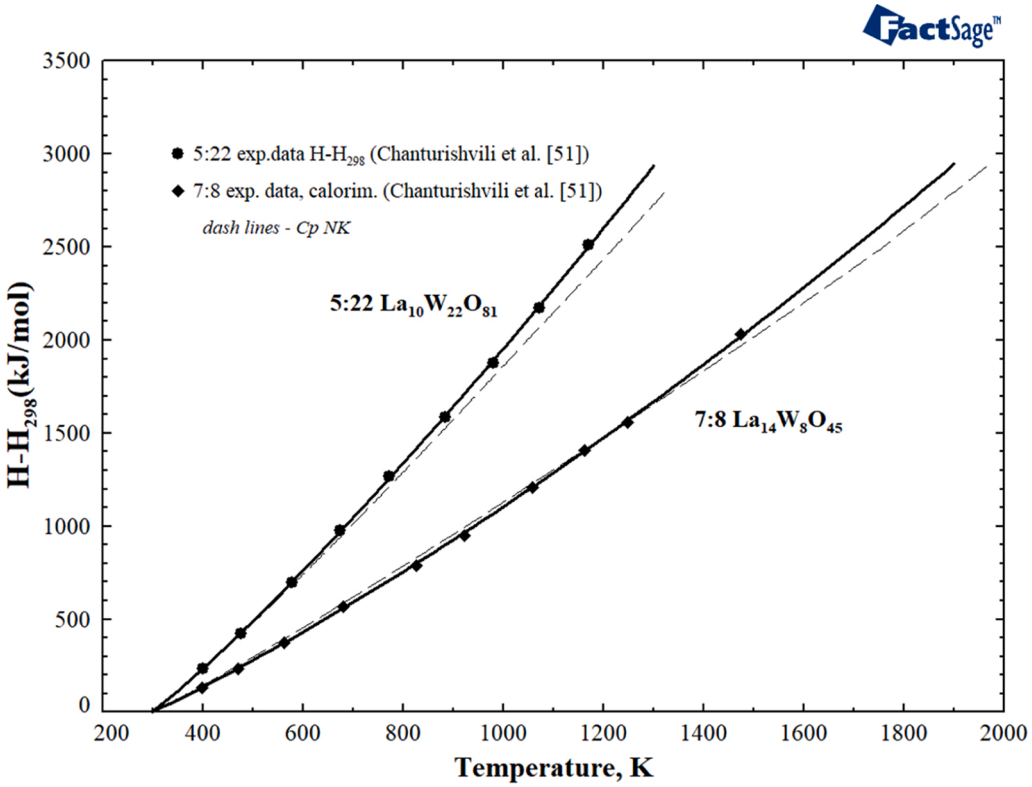

Fig. 5. Calculated enthalpy increment (solid line) of compounds 5:22 and 7:8 ($La_{10}W_{22}O_{81}$ and $La_{14}W_8O_{45}$) compared with the experimental data [51] and Neumann-Kopp approach (dashed line).

modification was identified to have a monoclinic structure, and the structure type of the high temperature phase could not be determined using the XRD data [41]. According to the literature, this transition is accompanied by neglectable changes of the structure [29]. Nassau et al. [41] called it as "non-destructive" phase transition with relatively minor rearrangement of atoms. Unfortunately, no data on the transition enthalpy of this transformation were found in the literature concerning tungstates of the lanthanides or even for the molybdates, which are iso-structural to $Ln_2(WO_4)_3$ [41,85]. Therefore, the transition enthalpy of $La_2(WO_4)_3$ at 1303 K was estimated to be 1.84 kJ/mol using the transition entropy of WO_3 at 1050 K.

The heat capacity of the compound 1:3 was obtained by calorimetric measurements [51]. The calculated enthalpy increment is presented in Fig. 6, whereas the heat capacity data are summarised in Fig. 7. The Cp data published in [86] were excluded due to their inconsistency with other data. The estimated values from the database aiMP (ab-initio Material Project compound database) [87] and the Neumann-Kopp data are given for comparison.

The present optimised values of the standard formation enthalpy are compared in Table 5 with the data derived in the thermodynamic data collections [58,87,88]. Plyuschev et al. [86,89] estimated $\Delta_f H^\circ_{298}$ and S°_{298} by comparative analysis of the thermodynamic data of similar compounds (sulphates, chlorides or tungstates of related metals). Chentsov [90] used the available EMF data to derive the thermodynamic functions for tungstates of Sc, Y, La, Dy, i.e. the Gibbs energy of formation from the elements. These values can be compared with those obtained from the EMF measurements in the temperature range 1134–1196 K [56]. The latter data have been recalculated using the present thermodynamic data regarding the oxidation of La and W to La_2O_3 and WO_3, respectively, because the values used in [56] are not identical to those applied in the present dataset. The calculated Gibbs energy values are summarised in Fig. 8. As it was mentioned in the previous chapter, these G values are also given per mole of crystalline oxide, the reaction of formation can be written for any lanthanum tungstate as follows:

$$2mLa + nW + \frac{3}{2}(m+n)O_2 = (La_2O_3)_m(WO_3)_n$$

In case of a compound La_2O_3:WO_3=m:n, the presented Gibbs energy values are calculated from ΔG_f^{elem} divided by (m+n) for better representation.

6.3.3. Compound $La_2W_2O_9$ (La_2O_3:WO_3=1:2). The phase transformation of $La_2W_2O_9$ was observed in various thermal and structural studies [29,31,51,91,92], and the transformation temperature was reported to be in the temperature range of 1340–1362 K (Table 9). The structure of the low temperature (LT) phase was resolved by Laligant et al. [43] using ab initio from neutron diffraction data. This LT phase with triclinic structure transforms to the cubic high temperature phase [91]. The recent data regarding the transition temperature, 1350 K [91] and 1353 K on heating curve [92], respectively, agreed with those from the earlier studies on the phase diagram [29,31] (1348 K, 1340 K) and the calorimetric study [51] (1362 K). The transition enthalpy was calculated by numerical integration of the recorded DTA to be 27.5 kJ/mol [92]. However, the value from the calorimetric study of Chanturishvili et al. [51], 43.51 kJ/mol, was preferred in the present work in order to keep the consistency with the heat capacity data. The calculated enthalpy increment of $La_2W_2O_9$ is compared with the experimental data [51] in Fig. 6. The heat capacity (Fig. 7) was directly derived from these calorimetric data, whereby the heat capacity above the phase transition was approximated as a constant value in accordance with the data [51].

The thermodynamic data of the solid compound 1:2 ($\Delta_f H^\circ_{298}$, S°_{298}) were optimised (Tables 5-7) for the proper description of the phase

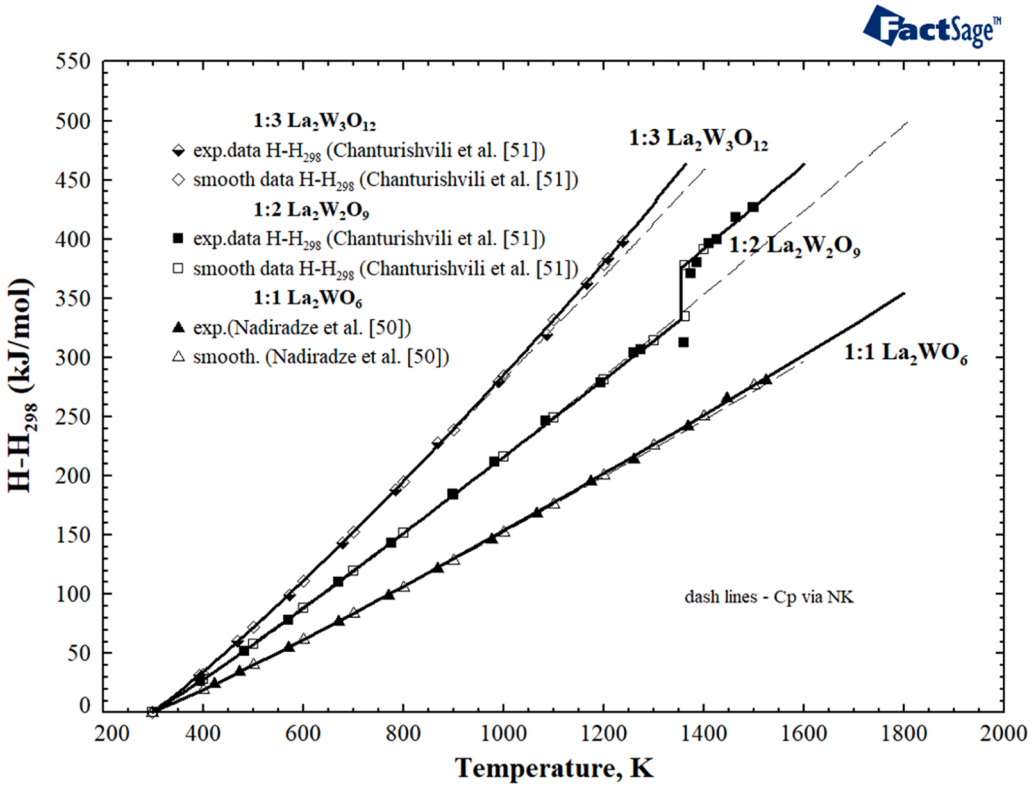

Fig. 6. Calculated enthalpy increment (solid line) of compounds 1:3, 1:2 and 1:1 ($La_2W_3O_{12}$, $La_2W_2O_9$ and La_2WO_6) compared with the experimental data [50,51] and Neumann-Kopp approach (dashed line).

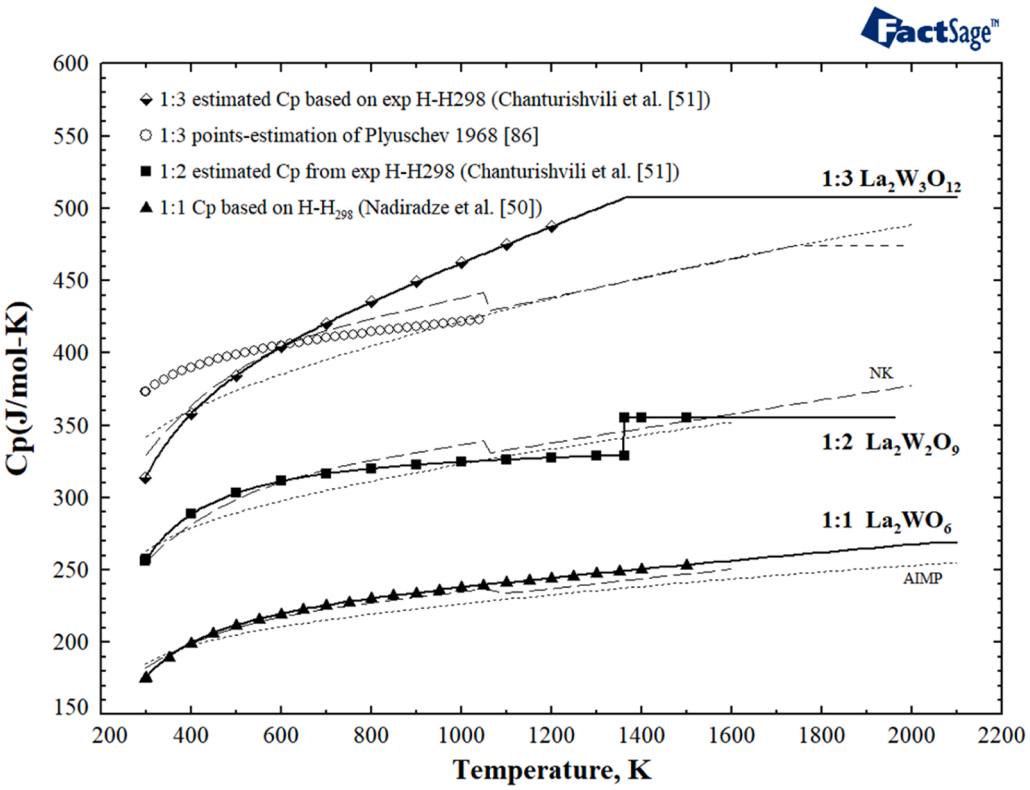

Fig. 7. Calculated heat capacity (solid line) of compounds 1:3, 1:2 and 1:1 ($La_2W_3O_{12}$, $La_2W_2O_9$ and La_2WO_6) compared with the experimental data [50,51,86], aiMP database [87] (dot line), and Neumann-Kopp approach (dashed line).

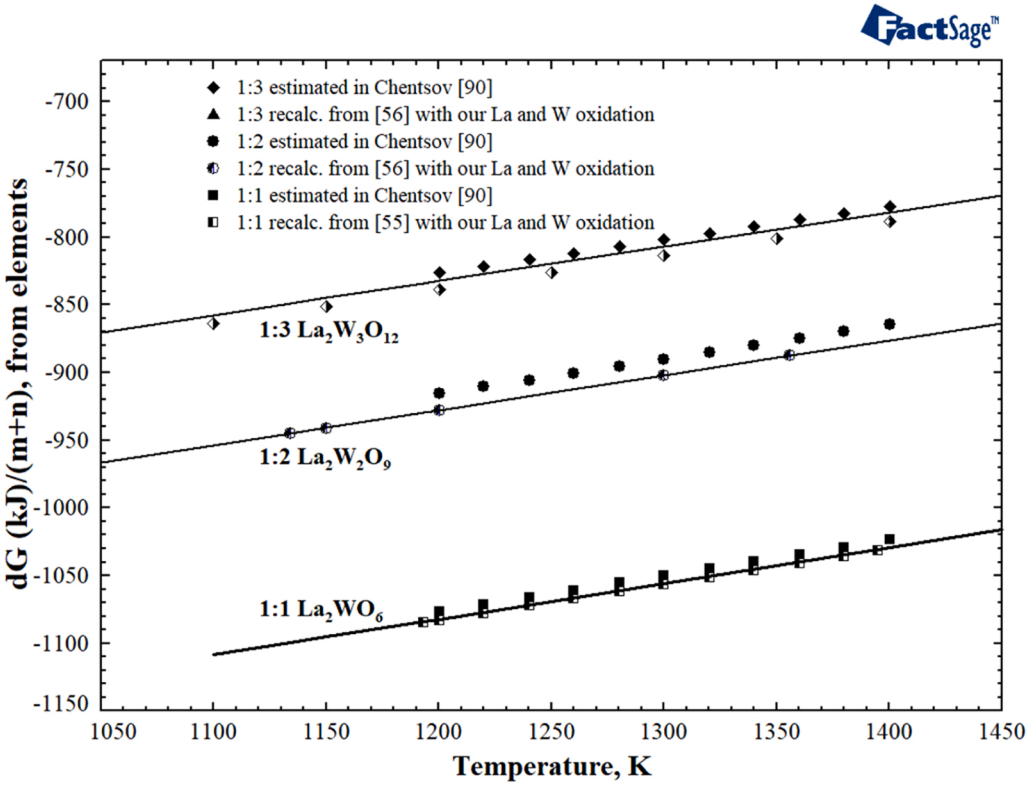

Fig. 8. Calculated Gibbs energy of formation of compounds 1:3, 1:2 and 1:1 ($La_2W_3O_{12}$, $La_2W_2O_9$ and La_2WO_6) from elements according to the reaction $2mLa + nW + \frac{3}{2}(m+n)O_2 = (La_2O_3)_m(WO_3)_n$ per mole of crystalline oxide, $\frac{\Delta G_f^{elem}}{m+n}$ compared with the experimental data [56,90].

equilibria along with the thermodynamic properties, namely (ΔG_f^{elem}), the latter values are calculated and compared with the available literature data (Fig. 8) [56,90].

6.3.4. Compound $La_{14}W_8O_{45}$ (La_2O_3:WO_3=7:8). Tyushevskaya et al. [28] reported the compound 7:8 as a low temperature phase of that with 1:1 ratio. Ivanova et al. [30] stated that 1:1 has a large homogeneous domain and that the compound 7:8 is an intermediate phase based on 1:1 solid solutions. However, Yoshimura et al. [35] indicated that their XRD data for 1:1 [30] consisted of a mixture of gamma-phase (one of the phase modification of the compound 1:1) and 7:8. Yoshimura could separate the data by annealing of fused samples. All reflections belonging to the compound 7:8 were indexed based on an orthorhombic cell, which can be indexed based on a pseudo-hexagonal cell with parameters a= 7.830 Å and C= 5.447 Å [35]. The compound of this stoichiometry has not been reported for other rare earths [4,31].

The structure of the sample with La_2O_3:WO_3= 7:8 was determined by synchrotron and laboratory X-ray, neutron, and electron diffraction data by Chambrier et al. [44]. It was reported that the refined composition is La_2O_3:WO_3= 9:10 instead of 7:8, but they were unable to see a small difference between both compositions during the synthesis. Since this compound melts incongruently, the exact formula does not affect the phase diagram of the system La_2O_3-WO_3. The compound with the composition 9:10 was synthetized using the self-flux method from the high-temperature solutions, but the formation of a single phase was not confirmed, as two phases were detected with XRD [93]. The compound 7:8 was investigated in the earlier structural [31,35], calorimetric [51] and EMF [56] studies, therefore, the compound $La_{14}W_8O_{45}$ is considered in the present work instead of that with the molar ratio 9:10.

According to Yoshimura et al. [31], no phase transitions were found for the compound $La_{14}W_8O_{45}$, and its incongruent melting point was reported to be below 1973 K (after thermal analysis - 1947 K).

In the present work, the thermodynamic function of 7:8 was modelled using the calorimetric [51] and the EMF data [56]. The heat capacity, the enthalpy increment, and the Gibbs energy of formation from La_2O_3 and WO_3 are plotted in Figs. 4, 5 and S4, correspondingly. The predicted stability of 7:8 is lower (Fig. S4) than that established in the EMF study. The values were obtained as a compromise considering both the phase equilibria and EMF data for the proper description of the melting behaviour of all compounds.

6.3.5. Compound La_2WO_6 (La_2O_3:WO_3=1:1). The solid-solid transition at 1713 K of the compound 1:1 from the low- to the high temperature modification with a tetragonal structure was found by thermal analysis and XRD study by Yoshimura et al. [31,35]. In these publications, the structure of the low-temperature phase (LT) was not known exactly in contrast to other tungstates with formula Ln_2WO_6. Chambrier et al. [45,94] established that La_2WO_6 (LT) crystallizes in an orthorhombic space group $P2_12_12_1$ by laboratory X-ray, neutron time-of-flight and electron diffraction data. Allix et al. [95] refined the structure of the high temperature (HT) modification using laboratory in situ high temperature X-ray powder diffraction and isolated this phase at room temperature by rapid quenching from 1873 K. Ab-initio structure determination was performed at room temperature by combining electron diffraction results with an analysis of synchrotron and neutron powder diffraction data by charge-flipping algorithm methods. The α-La_2WO_6 phase (HT) was found to crystallize in the $Pm2_1n$.

The solid-solid transformation between LT and HT phases was confirmed by the DSC measurement [95]. The enthalpy of transition was not known; therefore, this value was estimated using the data on other compounds Ln_2WO_6. The compounds with Ln=Eu and Nd have a similar structure. As reported by Allix et al. [95]: "These compounds typically present structural motifs based on the fluorite (CaF_2) or Scheelite ($CaWO_4$) structure type. Depending on the lanthanide (Ln) cation radius, three different space groups are commonly observed". Thus, their heats of transition were determined by calorimetry [96] and these values were 1.88 kJ/mol at 936 K and 0.22 kJ/mol at 936 K for Eu and Nd, correspondingly. In the present work, the transition data for the compound La_2WO_6 were estimated (0.447 kJ/mol at 1713 K [31]) based on the entropy change of the transitions between LT and HT phases of the compound Nd_2WO_6 (0.26 J/mol•K) considering the fact that the ionic radius of Nd is closer to that of La.

The heat capacity equation (Fig. 7) was adopted from the calorimetric measurement of Nadiradze et al. [50] and used in the present work without modifications. The enthalpy increment of the compound 1:1 is presented in Fig. 6. The standard formation enthalpy and standard entropy were optimised in accordance with the Gibbs energy data [55, 90] and the phase equilibria information. The calculated Gibbs energies of formation of the compound La_2WO_6 according to the reactions $2La + W + 3O_2 = (La_2O_3)_1(WO_3)_1$ and $La_2O_3 + W + 3O_2 = (La_2O_3)_1(WO_3)_1$ per mole of crystalline oxide, $\frac{\Delta G_f^{elem}}{1+1}$ and $\frac{\Delta G_f^{reac}}{1+1}$ are collected in Figs. 8 and 9, respectively. It should be noted that the second reaction of formation can be written for any lanthanum tungstate as follows:

$$mLa_2O_3 + nW + \frac{3n}{2}O_2 = (La_2O_3)_m(WO_3)_n$$

In case of a compound La_2O_3:WO_3=m:n, the presented Gibbs energy values (Fig. 9) are calculated from ΔG_f^{reac} divided by (m+n) for a better representation of various numbers.

6.3.6. Compound $La_6W_2O_{15}$ (La_2O_3:WO_3=3:2). The melting point of the compound $La_6W_2O_{15}$ is inconsistent in the literature: Ivanova et al. [30] reported incongruent melting at 2173 K, while Yoshimura et al. [31] and Yanovskii and Voronkova [32] found congruent melting at 2063–2065 K. According to the preliminary dilatometry measurements (Chapter 6.1), the melting temperature of 2158 K is adopted in the present study, although a more detailed study seems to be necessary for the compositions with high concentration of lanthanum oxide.

The structural, thermal and chemical stability and the conductivity of the compound $La_6W_2O_{15}$ were studied by Ivanova et al. [46] in order to clarify its impact on the performance of the LaWO-based membrane during manufacturing and operation when it can be segregated as a secondary phase. Since its conductivity is one to several orders of magnitude lower compared to the phase LaWO ($La_{6-x}WO_{12-\delta}$), this phase can compromise the performance of material of interest. Furthermore, the stability of this secondary phase plays for the overall stability of the LaWO membrane under relevant operation conditions (humidity, concentration of H_2, O_2, CO_2, etc). Therefore, the phase transformation of 3:2 were examined with HT XRD in the range from room temperature up to 1373 K supported by microstructure and conductivity measurements. Four stable structures were detected [46], the transformations were associated with strong variation in the microscopic thermal expansion coefficients. The first phase transitions (423–673 K) going over a metastable structure doesn't have an analogue in the literature. The transformations at 873–923 K and 1073–1173 K correspond to those reported earlier [30,31]. Based on DTA measurements, solid-solid transitions at 903 K and 1223 K and 903 K and 1203 K were reported by Rode et al. [29] and Ivanova et al. [30], respectively. Later, reversible thermal delays were observed by Yoshimura and Rouanet [31] at 892 K and 1202 K on heating and at 871 K and 1195 K on cooling. Similar results were obtained by Chambrier [47], 888 K and 1217 K on heating and 859 K and 1191 K on cooling, respectively. In the present work, the transformations at 903 K and 1203 K according to [29–31] were selected for the compound 3:2. The transition enthalpies and the heat capacity were taken from the calorimetric measurements [50].

The Gibbs energy of formation of the $La_6W_2O_{15}$ from La_2O_3, W and O_2 were calculated (Fig. 9) using the present dataset in good agreement with the EMF-based experimental values [55]. The heat capacity (Fig. 10) was modelled using the calorimetry measurements [50] of enthalpy increment (Fig. 11).

6.3.7. Compound $La_{10}W_2O_{21}$ (La_2O_3:WO_3=5:2). The compound 5:2 was considered by Ivanova et al. [30] and included into a solid solubility

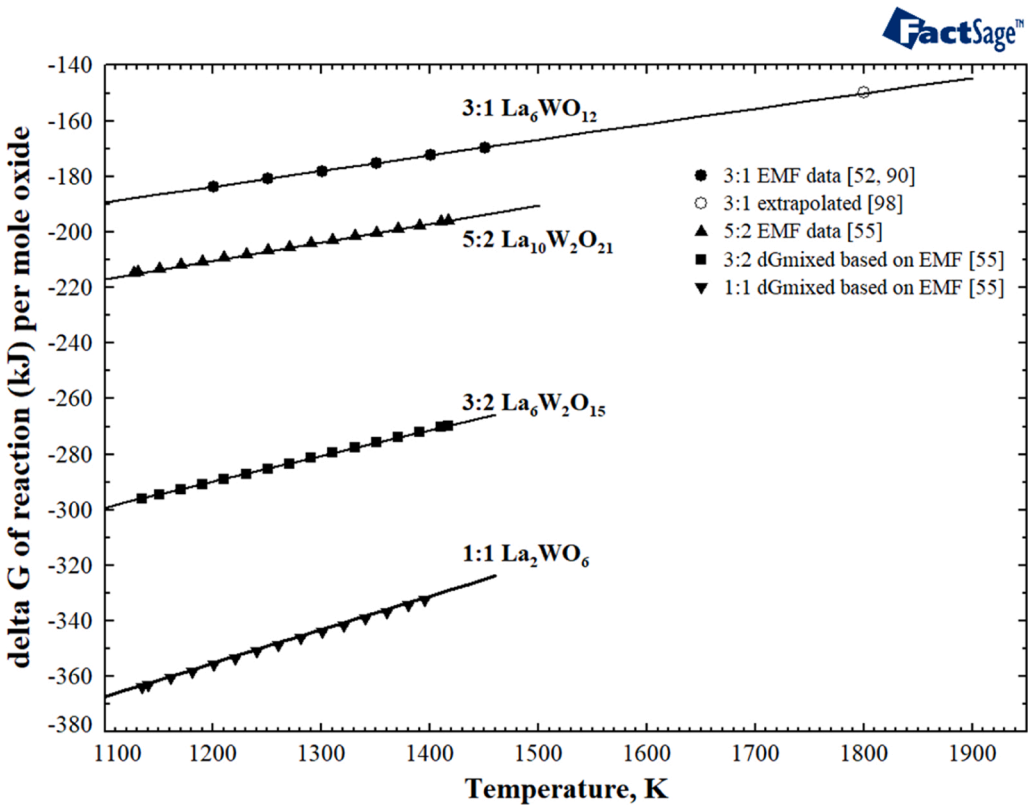

Fig. 9. Calculated Gibbs energy of formation (solid line) of the compounds 1:1, 3:2, 5:2 and 3:1 (La_2WO_6, $La_6W_2O_{15}$, $La_{10}W_2O_{21}$ and La_6WO_{12}) according to the reaction $mLa_2O_3 + nW + \frac{3n}{2}O_2 = (La_2O_3)_m(WO_3)_n$ per mole of crystalline oxide, $\frac{\Delta G_f^{reac}}{m+n}$.

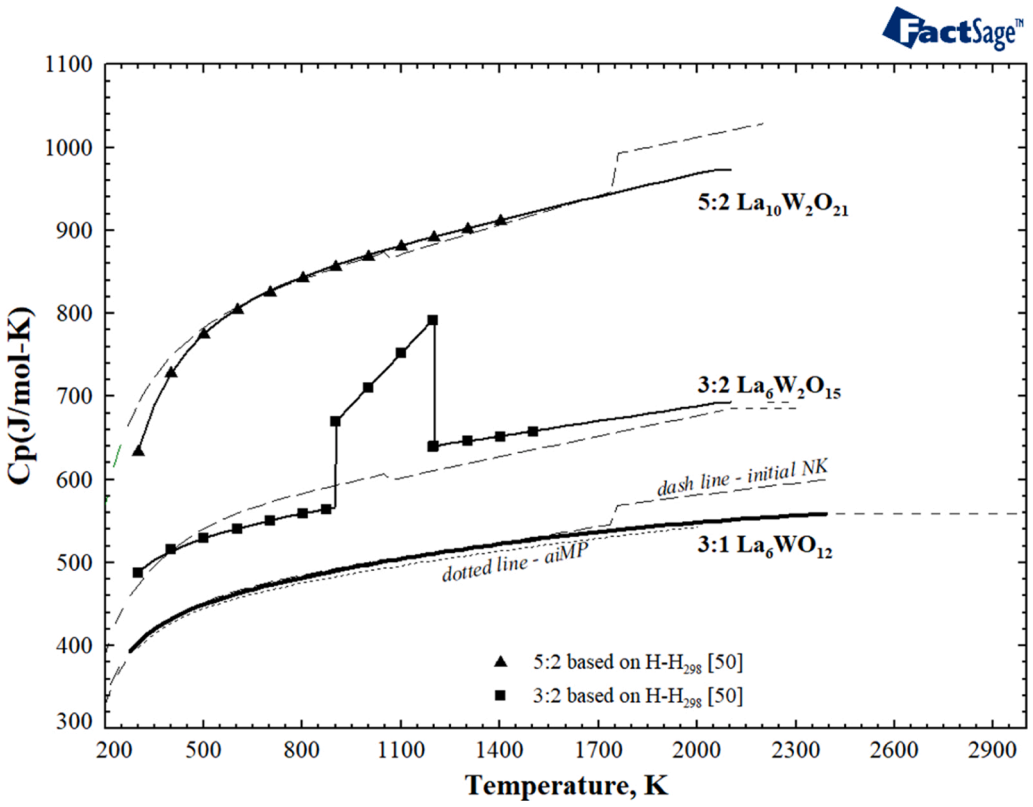

Fig. 10. Calculated heat capacity (solid line) of compounds 5:2, 3:2 and 3:1 ($La_{10}W_2O_{21}$, $La_6W_2O_{15}$ and La_6WO_{12}) compared with the experimental data [50] and Neumann-Kopp approach (dashed line).

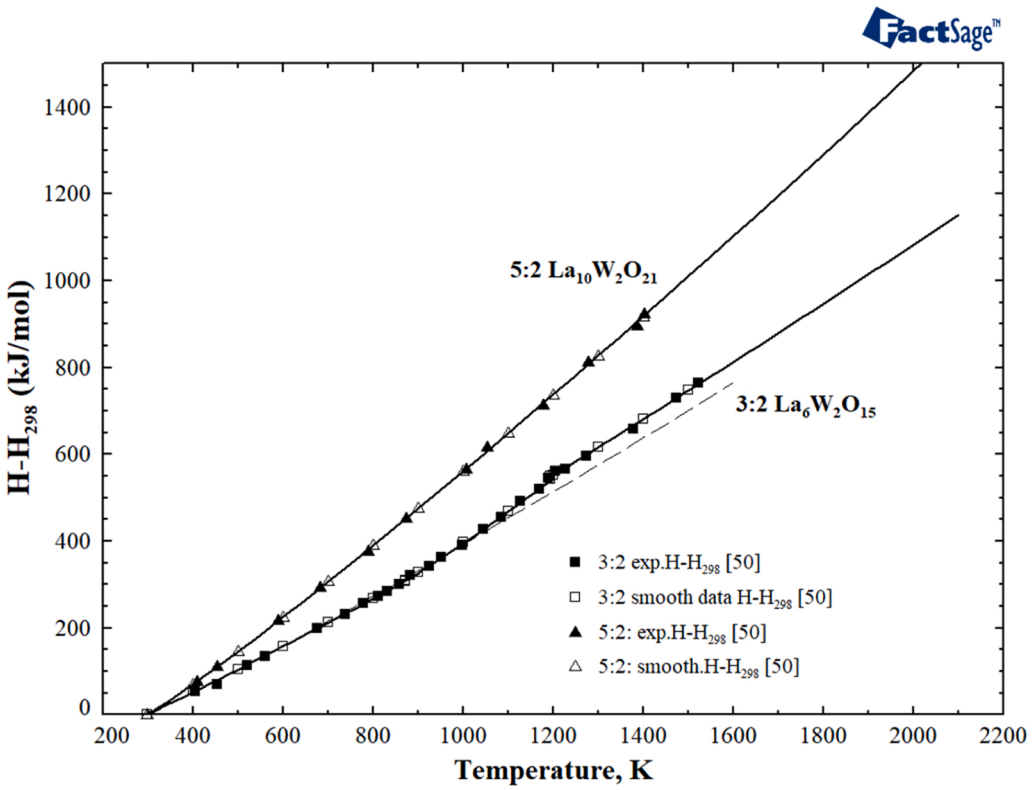

Fig. 11. Calculated enthalpy increment (solid line) of compounds 5:2 and 3:2 ($La_{10}W_2O_{21}$ and $La_6W_2O_{15}$) compared with the experimental data [50] and Neumann-Kopp approach (dashed line).

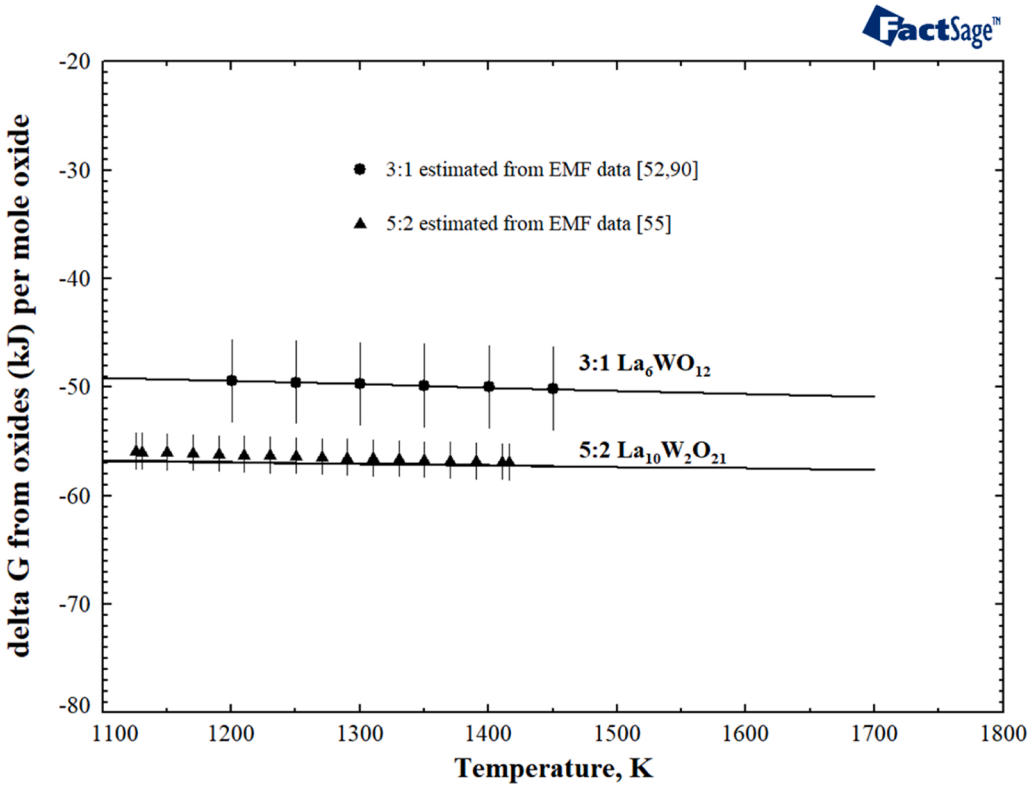

Fig. 12. Calculated Gibbs energy of formation of the compounds 3:1 and 5:2 (La_6WO_{12} and $La_{10}W_2O_{21}$) according to the reaction $mLa_2O_3 + nWO_3 = (La_2O_3)_m(WO_3)_n$ per mole of crystalline oxide, $\frac{\Delta G_f^{ox}}{m+n}$ in comparison with the literature data [55,90].

in the compositional range 0.7–0.75 mol fraction of La_2O_3. Later, this compound was investigated by Yoshimura et al. [31,36] who applied solid state reaction, co-fusion, annealing coupled with high temperature XRD in order to investigate the phase relations in the La_2O_3-rich part of the system, between the compounds 5:2 and 3:1. The compound 5:2 was identified to have a cubic fluorite structure with the superstructure lines that are characteristic for the pyrochlore-related fcc structure. It is stable up to 2043 K and appeared to decompose into the compound 3:1 (La_6WO_{12}) and the compound 3:2 ($La_6W_2O_{15}$) at higher temperatures. Similar results were obtained by Casteels et al. [34] who proposed a decomposition temperature of 2093 K.

The Gibbs energy of the stoichiometric compound $La_{10}W_2O_{21}$ is used for the description of the phase LaWO (Chapter 4.3). The coefficients for the temperature dependence of heat capacity were adopted from the calorimetric data [50]. The heat capacity of 5:2 and enthalpy increment are plotted in Figs. 10 and 11, respectively. To provide the stability of the phase from room temperature to the decomposition, the $\Delta_f H^{\circ}_{298}$, S°_{298} were optimised in accordance with the EMF and phase diagram data. The calculated Gibbs energies of formation from the mixture La_2O_3, W, O_2 and from the end-member oxides are presented in Figs. 9 and 12, correspondingly, in comparison with the literature data [55].

6.3.8. Compound La6WO12 (La2O3:WO3=3:1). Chang and Philipps [49] prepared in 1964 the compound 3:1 by solid-state reaction of the oxides at temperatures above 1673 K in air to prevent volatilisation of WO_3. The compound obtained melts at 2323 ± 20 K, the DTA study did not show any heat effect up to 1673 K. According to Chang and Philipps [49]: "The compound can lose oxygen when heated above 1073 K under vacuum without change in structure but with colour changes toward grey. Reheating in air restores the original colour (white)". The solidification temperature was determined to be 2233 K for the lanthanum containing compound in the series of rare-earth tungstates R_6WO_{12} by Foex in 1967 [97]. The structure of 3:1 was indexed as fcc unit cell and classified by Chang and Phillips [49] as disordered pyrochlore (or ordered defect fluorite) with a= 11.18 Å.

On the phase diagram published by Ivanova et al. [30] this compound La_6WO_{12} was introduced to be a stable phase from low temperature up to the congruent melting point at ≈ 2423 K. Later, Casteels et al. [34] and Yoshimura et al. [31,36] reported this phase appears at high temperatures only, with stability ranges of 2093–2313 K and 2013–2233 K, respectively.

Similar to the previous chapter, the discussion on the solubility based on the compounds 5:2 and 3:1 is presented in Chapters 2.3 and 6.3. In the present work, this solution phase is modelled using the Compound Energy Formalism (Chapter 4.3). However, the thermodynamic properties of the stoichiometric compound were generated in order to provide a starting dataset for modelling the LaWO phase.

In the present work, the heat capacity of the compound 3:1 was generated from the corresponding data of the pure oxides using Neumann-Kopp's rule with small modifications (solid line in Fig. 10), since no experimental data are available in the literature. The Cp values are compared with the ab-initio data from the aiMP database [87]. The Gibbs energy of the compound was modelled to enable the prediction of the stability range of the compound 3:1 at higher temperatures only. The EMF measurements of Chentzov et al. [52,90] who determined the Gibbs energy of formation (ΔG_f^{reac}) according to the reaction $3La_2O_3+W+3/2O_2=La_6WO_{12}$ in the temperature range 1200–1450 K) were used to establish the thermodynamic function of this compound. Fig. 9 presents the calculated Gibbs energy of formation from La_2O_3, W, O_2 related to one mole of oxides, namely $\frac{\Delta G_f^{reac}}{3+1}$. The value of the Gibbs energy for the same reaction at 1800 K was extrapolated by Levitskii et al. [98] using the thermodynamic data on similar tungstates of rare earth oxides. This value agrees with the experimental and calculated data. The thermodynamic values (standard formation enthalpy, standard entropy and the formation enthalpy from the oxides) were derived in those works [52,90] and compared with the optimised values in Tables 5–7.

Summarising the thermodynamic data on 3:1 (Tables 5–8), the enthalpy and entropy values agree well with the available experimental and estimated information. The calculated enthalpy of formation from oxides ($\Delta H^{ox}_{298,f}$) differs from those in the literature [52,90], because these authors derived the thermodynamic properties of 3:1 based on their EMF data related to the reaction from La_2O_3, W, O_2 using different thermodynamic information on oxides and elements. Specifically, the Gibbs energy of W oxidation differs from that used in the book [58] and in the present work. Thus, the Gibbs energy of formation from oxides (ΔG_f^{ox}) cannot be compared directly with the estimations published in [52,90]. Therefore, this Gibbs energy of the reaction ($3La_2O_3+WO_3=La_6WO_{12}$) is recalculated using the EMF data [52,90] for the reaction from La_2O_3, W, O_2 combined with the corrected values for the W oxidation ($W+3/2O_2=WO_3$). After this re-calculation, the values ΔG_f^{ox} agree with the literature data [52,90]. The comparison is shown in Fig. 13, the corresponding Gibbs energies of the reaction from oxides are given per mole oxide similar to the reaction from La_2O_3, W, O_2.

6.4. Phase equilibria of the La_2O_3-WO_3 system

The thermodynamic dataset for the system La_2O_3 and WO_3 was generated using the available literature data on phase equilibria and thermodynamic properties. The Gibbs energies for eight stoichiometric compounds and solution phases were obtained in good agreement with the available experimental information. The optimised parameters in the liquid and solid phases allow the accurate description of the phase equilibria as well as other properties.

The formation enthalpy from the end-member oxides, La_2O_3 and WO_3, can be calculated for any lanthanum tungstate by the following formula: $mLa_2O_3 + nWO_3 = (La_2O_3)_m(WO_3)_n$. The calculated data at 298 K are summarised in Table 8 and Fig. 13 in comparison with the selected experimental data. The value of ΔH_f^{ox} are consistent with each other, and the minimum of the enthalpy of formation is located at the compound 7:8. Using the optimised parameter of the liquid phase, the enthalpy of mixing was predicted at 2673 K (Fig. 14). The calculated value of ΔH_{mix}^{liq} is asymmetric and has a V-shape with the minimum at 0.44 mol fraction of La_2O_3 indicating a tendency to short-range ordering at this composition.

The literature data on phase equilibria were critically assessed. The solid-liquid equilibria reported in [29–32] were considered by optimisation of the thermodynamic parameters in the system. In the La_2O_3-rich concentration range, the data published by Yoshimura and Rouanet [31] were preferred. Fig. 15 shows the calculated phase equilibria in the system La_2O_3-WO_3. Additionally, the calculated phase diagram in °C is added to Supplementary (Fig. S5). The invariant points (solid-solid and solid-liquid transitions) are summarised in Table 9.

In agreement with the literature, the compounds 5:22, 1:2, 1:1, and 3:2 melt congruently, while the compositions 1:3 and 7:8 undergo peritectic decomposition at the corresponding temperatures. The melting temperature of $La_6W_2O_{15}$ was optimised to be close to the experimentally found value of 2158 K considering other thermodynamic properties and the melting behaviour of the neighbour compounds. The calculated liquidus line at high amount of La_2O_3 is considered as compromise between Yoshimura [31] and Ivanova [30]. However, further experimental study may be needed to solve these contradictions.

The formation of the solid solution in the concentration range 0.71–0.75 mol fraction of La_2O_3 is intensively discussed in the literature. The compound 3:1 is reported in the literature [30] to be a part of the solid solution that was proposed in the compositional range 0.7–0.75 mol fraction of La_2O_3 including the chemical composition of the compound 5:2 (0.714 mol fraction La_2O_3) as well. In opposite to this, Yoshimura et al. [36] suggested a discontinuous phase change between 5:2 and 3:1 in the samples annealed at 1673 K. According to the

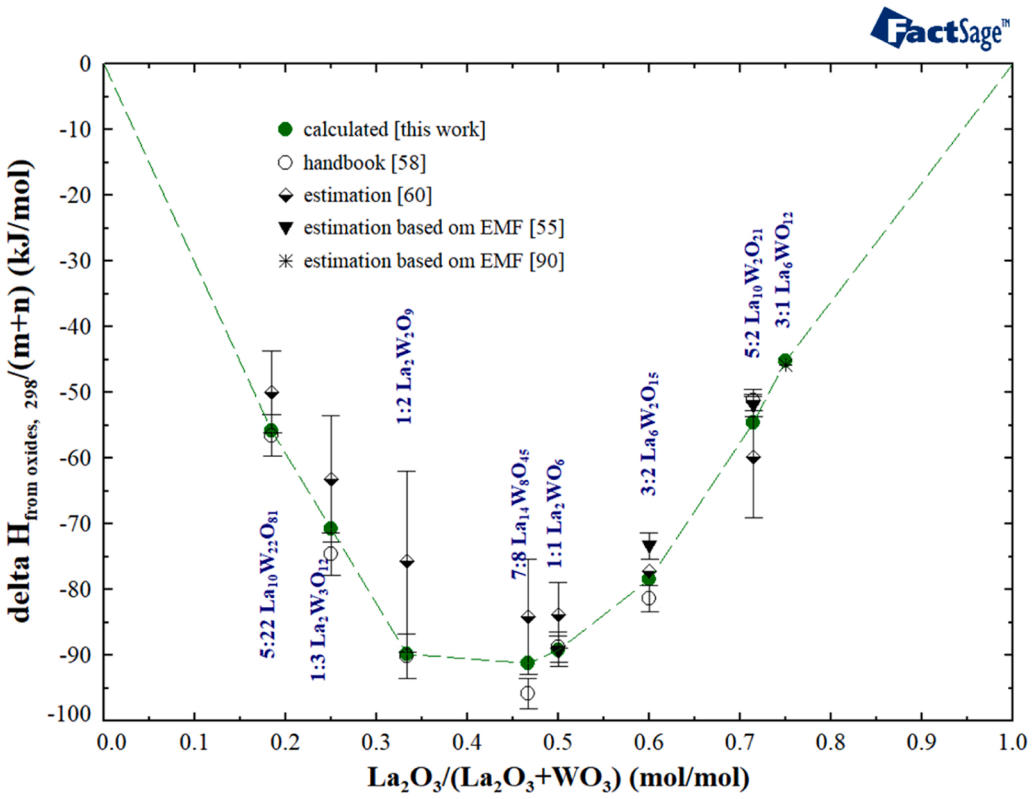

Fig. 13. Formation enthalpy of lanthanum tungstates from oxides at 298 K according to the reaction: $mLa_2O_3 + nWO_3 = (La_2O_3)_m(WO_3)_n$ per mole of crystalline oxide, $\frac{\Delta H_f^{ox}}{m+n}$, in comparison with the experimental data from the literature.

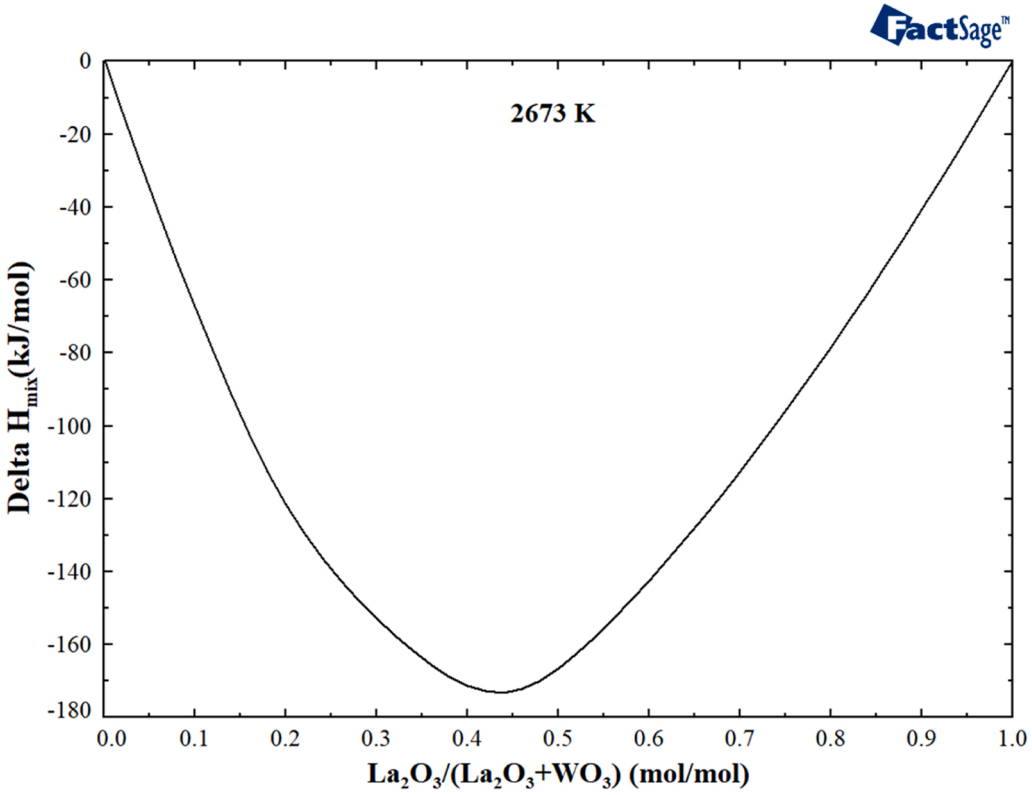

Fig. 14. Calculated mixing enthalpies of the liquid phase La_2O_3-WO_3 at 2673 K.

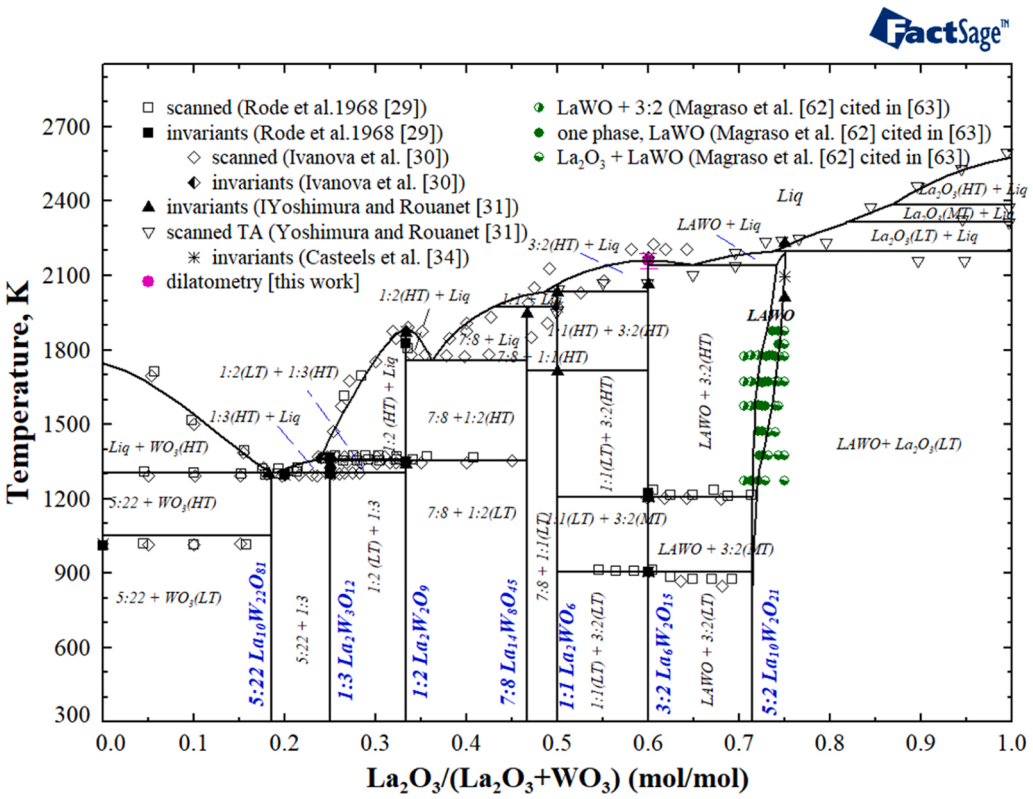

Fig. 15. Calculated phase diagram in the system La_2O_3-WO_3 along with the experimental data.

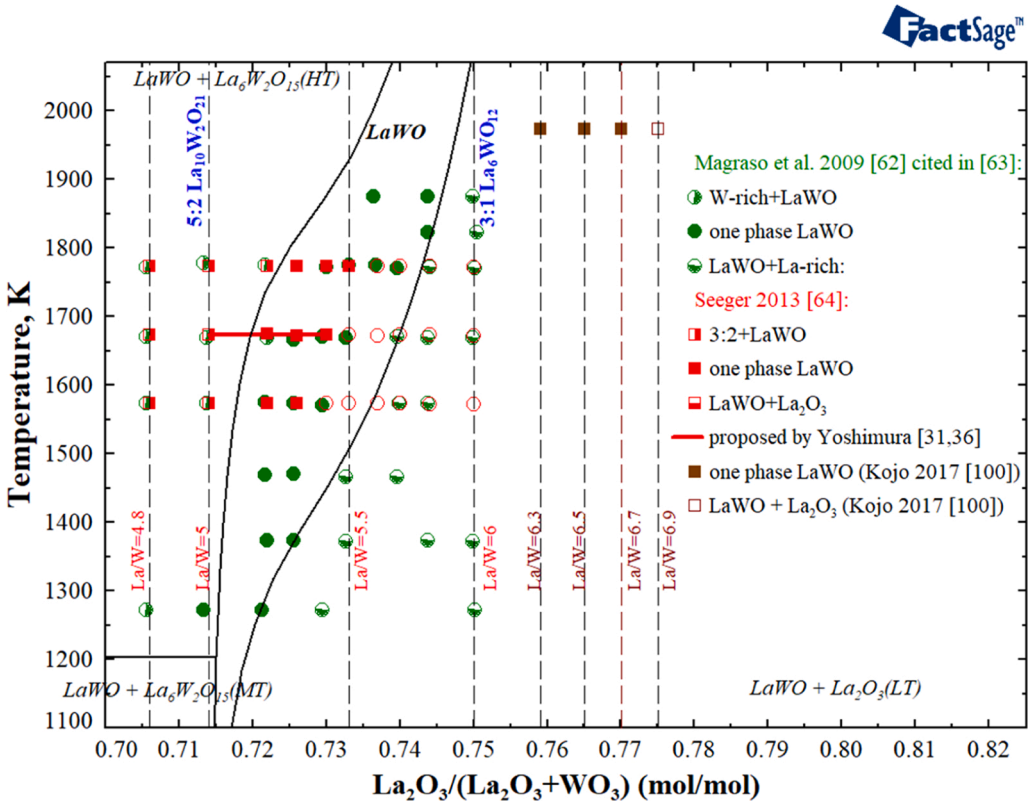

Fig. 16. The part of the calculated phase diagram of the system La_2O_3-WO_3 illustrating the solid solution phase LaWO in comparison with the available experimental data.

temperature dependence of the cubic lattice parameters, both phases coexist between 2013 K and 2073 K. Later, Chambrier et al. [48] analysed the structural properties of the compound 5:2 to understand, whether the compounds 5:1 and 3:1 having similar structure are individual compounds or belong to the solid solution. The structure of the powder sample of 5:2 and the quenched sample 3:1 were confirmed to be very similar, so the formation of a very limited solution based on $(La_{6-x}W_x)LaWO_{13.5+1.5x}V_{2.5-1.5x}$ with V – vacancy, $x = 1/3 \pm\delta$, and δ very small was proposed. At $x = 1/3$ the formula corresponds to the ratio La/W= 5 as in the compound 5:2.

The structure of this phase was proved more accurately using modern techniques by Magraso et al. [62], by Scherb et al. [19]. According to the XRD and neutron scattering data, the composition 3:1 belongs to the solid solution existing in the compositional range 0.714–0.75 mol fraction of La_2O_3. Similar results were obtained by Seeger et al. [12,64]. The possible extension of this solid solution was reported by Kojo et al. [100] who synthesised the single phase patterns in the range La/W= 6.3–6.7 (0.759–0.77 mol fraction of La_2O_3) by the citric acid complexation method with high-temperature sintering at around 1973 K. Thus, the field of LaWO should strongly incline towards the La_2O_3-rich compositions. Therefore, the data [62,64] were favoured to introduce the solid solution LaWO instead of two stoichiometric compounds, $La_{10}W_2O_{21}$ and La_6WO_{12} (Fig. 15). The stability range is strongly dependent on the temperature and composition. According to the literature, this phase with one structure extends in air in the temperature range from 1273 K to 1873 K. The Gibbs energies of the solution components and the corresponding interaction parameters were optimised considering the solubility area extending from 0.714 to 0.75 mol fraction of La_2O_3, that corresponds to the compositions from $La_{10}W_2O_{21}$ to La_6WO_{12} or to the ratio La/W from 5 to 6, respectively (Fig. 16). The predicted phase fields containing one phase or two phases agree with the equilibrium measurements presented by Magraso et al. [62,63]. The calculated phase boundaries bend from $La_{10}W_2O_{21}$ to La_6WO_{12} in the temperature range under consideration.

The theoretical numbers of oxygen vacancies and tungsten on the lanthanum sites in the solid solution were considered according to the structure studies [63]: the amount of W doped on the La sites ($W_{La}^{\bullet\bullet\bullet}$) decreases with increasing amount of La_2O_3 or with increasing ratio La/W. The relative amount of this defect ($W_{La}^{\bullet\bullet\bullet}$) can be related to the relative amount of the solution components with W (WO and WVa). The amount of oxygen vacancies, which are responsible for the conductivity of this phase, can be reproduced by the relative amount of the species LaVa and WVa in the range of solid solubility from 0.714 to 0.75 mol fraction of La_2O_3. The isothermal distribution of all solution constituents can reproduce the defect structure of this phase. Using the present dataset, the amount of all solution species was calculated at 1773 K (Fig. S6 in Supplementary). From these data the amount of the tungsten on the La position (W_{La}) as a function of the mole fraction of La_2O_3 were calculated based on the formula $La_{26.67}W_4(W, La)_{1.33}(O)_{54}(O, Va)_2$ (Fig. 17). The amount of vacancies (Va) was directly derived from the calculated mole fraction of LaVa and WVa. The results obtained show a good agreement with the theoretical values, indicating the applicability of the model.

Thus, the proposed model is able to describe the solid solubility between the compounds 5:2 and 3:1 in accordance with the available structural data. This model was validated depending on the composition and temperature. This description can be used for understanding the crystal structure of this solution and for prediction of its stability. The present modelling doesn't directly consider the partial pressure of oxygen so far. Since the dependence on the partial pressure of oxygen is crucial for the manufacturing and application of such materials, further improvement and modification of the solution model is necessary. For this purpose, measurements under reducing atmosphere and in pure oxygen would be desired to modify/validate the solution model and to understand the stability of this phase under different operation conditions.

The solid solutions based on La_2O_3 were mentioned in one paper

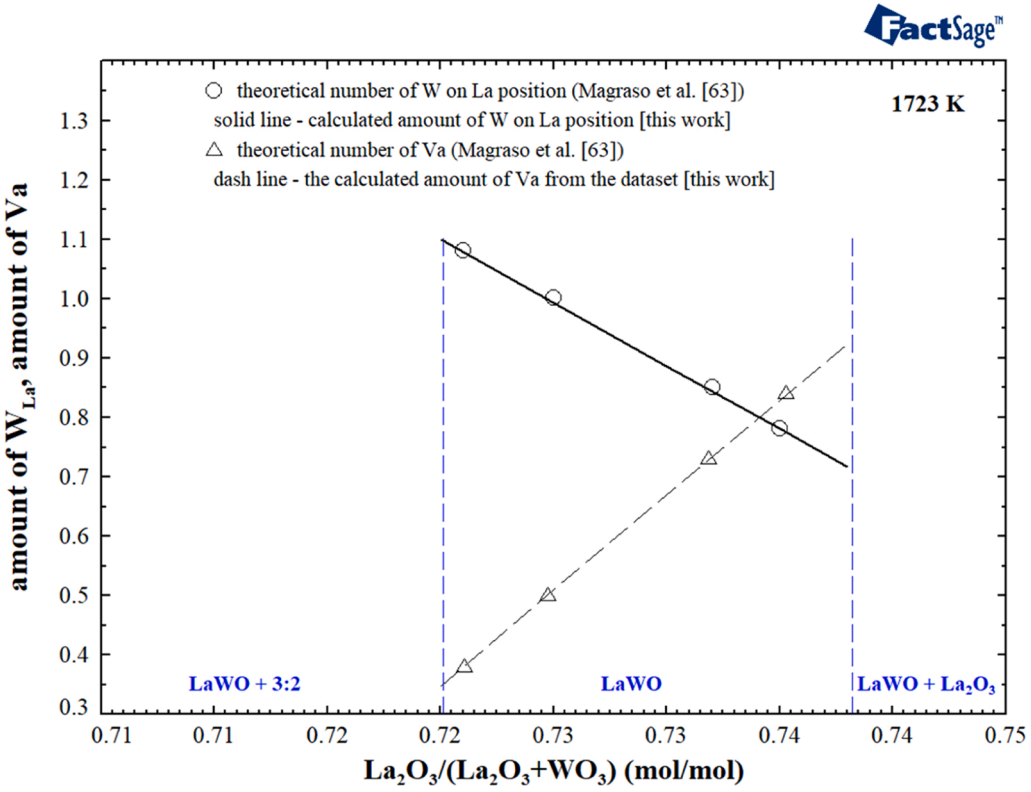

Fig. 17. Calculated numbers of W on the position of La (W_{La}) and vacancies (Va) as a function of the mole fraction of La_2O_3 in LAWO, based on the formula $La_{26.67}W_4(W, La)_{1.33}(O)_{54}(O, Va)_2$ at 1773 K. The theoretical values are taken from Magraso et al. [63].

[31], and since no further structural information is available, these phases are omitted in the present work.

In conclusion, it should be noted that the present dataset and the model used were not validated directly in terms of the dependence on the partial pressure of oxygen due to the lack of experimental data. However, the present database describes the thermodynamic properties as a function of chemical composition and temperature in a good agreement with the available independent experimental data, including phase equilibria, structure and calorimetric data. The selected models for description of liquid and solid solution phases and the appropriate optimised parameters were able to provide a reliable and reasonable description of the thermodynamics of the oxide system La_2O_3-WO_3.

6.4.1. *Equilibrium with the gas phase*

The high-temperature KEMS measurements by Casteels et al. [34] allowed to determine the partial pressure of various species over pure La_2O_3 and the mixtures in the La_2O_3-WO_3 system. Using the present dataset, the partial pressure of the corresponding gaseous species can be calculated. Thermodynamic data on all gas species in the La-W-O system were taken from the commercial database SGPS [69].

The values of LaO pressure will mainly be determined by the formation enthalpy of LaO(g), which is reported to be from −113 to −126 kJ/mol in the literature. Thermodynamic data on the gas species in the La-O system were presented by Heyrman et al. [101] based on mass-spectrometric measurements and critical analysis performed by Younes [102]. The proposed values [101] for the species LaO(g) and La (g) are adopted in the SGPS database (-114.2 kJ/mol), that is used here in combination with the present dataset for the condensed phases. The calculated pressure of LaO over the pure lanthanum oxide (green line, figure S7 in Supplementary) are compared with the selected literature data [34,103,104]. In the case of the enthalpy value of −125.5 kJ/mol based on the mass-spectrometry and mass effusion measurements by Ackermann and Rauh [103] the calculated pressure of LaO(g) is closer to the experiments (black line in Fig. S6). However, the data on the gas phase is beyond the scope of the present work, therefore, the data from the commercial database SGPS will be used in the present work without modifications.

The calculated values of partial pressure of LaO (gas) over La_2O_3 and $La_{10}W_2O_{21}$ are compared with the measured data [34] (Fig. S8). It should be noted that the calculations were performed at a fixed activity of W(solid)= 1 to reproduce the experimental conditions (tungsten cell for KEMS measurements). So, the agreement is reasonable, although the exact composition wasn't given in the literature.

7. Conclusions

The system La-W-O was thermodynamically considered focussing on the core system La_2O_3-WO_3. Thermodynamic properties and phase equilibria in this oxide system were critically assessed to generate a new thermodynamic dataset containing eight stoichiometric solid compounds with various oxide ratio La_2O_3:WO_3, the liquid phase and the solid solubility phase based on the compound 5:2. All phases in the system have been described using the appropriate models, and thermodynamic parameters have been optimised to provide a good agreement with the available experimental information on phase equilibria and thermodynamic properties. The dataset obtained provides a proper description of the thermodynamic properties of the system under consideration depending on temperature and chemical composition. This allows the use of the database for calculation and prediction of the stability and phase equilibria depending on chemical composition and temperature. By this, the that is helpful for development of the ceramic materials based on the La_2O_3-WO_3 system is essentially aided.

CRediT authorship contribution statement

Ivanova Mariya: Writing – review & editing, Conceptualization, Investigation, Writing – original draft. **Dmitry Sergeev:** Writing – review & editing, Investigation. **Michael Müller:** Writing – review & editing, Supervision, Funding acquisition. **Elena Yazhenskikh:** Writing – review & editing, Writing – original draft, Visualization, Validation, Methodology, Investigation, Conceptualization.

Declaration of Competing Interest

The authors declare that they have no known competing financial interests or personal relationships that could have appeared to influence the work reported in this paper.

Acknowledgments

This work was supported by the Helmholtz Research Program "Materials and Technologies for the Energy Transition" (MTET). The publication is also funded by the German Research Foundation (Deutsche Forschungsgemeinschaft DFG) - 491111487. Open Access funding enabled and organized by project DEAL.

Appendix A. Supporting information

Supplementary data associated with this article can be found in the online version at doi:10.1016/j.jallcom.2025.182973.

References

[1] M.E. Ivanova, R. Peters, M. Müller, S. Haas, M.F. Seidler, G. Mutschke, O. Guillon, Technological pathways to produce compressed and highly pure hydrogen from solar power, Angew. Chem. Int. Ed. 62 (32) (2023) e202218850, https://doi.org/10.1002/anie.202218850.

[2] J. Kim, S. Sengodan, S. Kim, O. Kwon, Y. Bu, G. Kim, Proton conducting oxides: a review of materials and applications for renewable energy conversion and storage, Renew. Sustain. Energy Rev. 109 (2019) 606–618, https://doi.org/10.1016/j.rser.2019.04.042.

[3] N. Diot, O. Larcher, R. Marchand, J.Y. Kempf, P. Macaudière, Rare-earth and tungsten oxynitrides with a defect fluorite-type structure as new pigments, J. Alloy. Compd. 323-324 (2001) 45–48, https://doi.org/10.1016/S0925-8388(01)00999-9.

[4] G.J. McCarthy, R.D. Fisher, G.G. Johnson Jr., G. C.E, *crystal chemistry and compound formation in the systems rare earth sesquioxide-wo3.* in National Bureau Standards Special Publication, Solid State Chemistry, Proceedings of the 5th Materials Research Symposium, 1972, pp. 397–411.

[5] T. Shimura, S. Fujimoto, H. Iwahara, Proton conduction in non-perovskite-type oxides at elevated temperatures, Solid State Ion. 143 (1) (2001) 117–123, https://doi.org/10.1016/S0167-2738(01)00839-6.

[6] R. Haugsrud, C. Kjølseth, Effects of protons and acceptor substitution on the electrical conductivity of La_6WO_{12}, J. Phys. Chem. Solids 69 (7) (2008) 1758–1765, https://doi.org/10.1016/j.jpcs.2008.01.002.

[7] R. Haugsrud, in: H.Y.W. Vielstich, H.A. Gasteiger (Eds.), New high-temperature proton conductors for fuel cells and gas separation membranes, 5, Handbook of Fuel Cells - Fundamentals, Technology and Applications, John Wiley & Sons Chichester, UK, 2009.

[8] R. Haugsrud, H. Fjeld, K.R. Haug, T. Norby, Mixed ionic and electronic conductivity of undoped and acceptor-doped Er_6WO_{12}, J. Electrochem. Soc. 154 (1) (2007) B77–B81, https://doi.org/10.1149/1.2374948.

[9] V. Stournari, W. Deibert, M.E. Ivanova, C. Krautgasser, R. Bermejo, J. Malzbender, Mechanical properties of tape casted lanthanum tungstate for membrane substrate application, Ceram. Int. 42 (14) (2016) 15177–15182, https://doi.org/10.1016/j.ceramint.2016.06.109.

[10] S. Escolástico, V.B. Vert, J.M. Serra, Preparation and characterization of nanocrystalline mixed Proton−Electronic conducting materials based on the system Ln_6WO_{12}, Chem. Mater. 21 (14) (2009) 3079–3089, https://doi.org/10.1021/cm900067k.

[11] S. Escolástico, C. Solís, J.M. Serra, Hydrogen separation and stability study of ceramic membranes based on the system Nd_5LnWO_{12}, Int. J. Hydrog. Energy 36 (18) (2011) 11946–11954, https://doi.org/10.1016/j.ijhydene.2011.06.026.

[12] J. Seeger, Entwicklung protonenleitender Werkstoffe und Membranen auf Basis von Lanthan-Wolframat für die Wasserstoffabtrennung aus Gasgemischen, 188, Bochum University: Schriften des Forschungszentrums Jülich, Reihe Energie & Umwelt; Bd., 2013, p. 130.

[13] E. Quarez, K.V. Kravchyk, O. Joubert, Compatibility of proton conducting La_6WO_{12} electrolyte with standard cathode materials, Solid State Ion. 216 (2012) 19–24, https://doi.org/10.1016/j.ssi.2011.11.003.

[14] D. van Holt, E. Forster, M.E. Ivanova, W.A. Meulenberg, M. Müller, S. Baumann, R. Vaßen, Ceramic materials for H_2 transport membranes applicable for gas separation under coal-gasification-related conditions, J. Eur. Ceram. Soc. 34 (10) (2014) 2381–2389, https://doi.org/10.1016/j.jeurceramsoc.2014.03.001.

[15] E. Forster, D. van Holt, M.E. Ivanova, S. Baumann, W.A. Meulenberg, M. Müller, Stability of ceramic materials for H_2 transport membranes in gasification environment under the influence of gas contaminants, J. Eur. Ceram. Soc. 36 (14) (2016) 3457–3464, https://doi.org/10.1016/j.jeurceramsoc.2016.05.021.

[16] W. Deibert, M.E. Ivanova, W.A. Meulenberg, R. Vaßen, O. Guillon, Preparation and sintering behaviour of $La_{5.4}WO_{12-\delta}$ asymmetric membranes with optimised microstructure for hydrogen separation, J. Membr. Sci. 492 (2015) 439–451, https://doi.org/10.1016/j.memsci.2015.05.065.

[17] W. Deibert, M.E. Ivanova, K. Ran, J. Mayer, W.A. Meulenberg, Up-scaling and processing related characterisation of hydrogen permeation membranes based on pristine and mo substituted $La_{28-x}W_{4+x}O_{54+1.5x}$, J. Eur. Ceram. Soc. 43 (1) (2023) 121–129, https://doi.org/10.1016/j.jeurceramsoc.2022.09.033.

[18] M.E. Ivanova, W. Deibert, D. Marcano, S. Escolástico, G. Mauer, W. A. Meulenberg, O. Guillon, Lanthanum tungstate membranes for H_2 extraction and CO_2 utilization: fabrication strategies based on sequential tape casting and plasma-spray physical vapor deposition, Sep. Purif. Technol. 219 (2019) 100–112, https://doi.org/10.1016/j.seppur.2019.03.015.

[19] T. Scherb, S.A.J. Kimber, C. Stephan, P.F. Henry, G. Schumacher, S. Escolastico, J. Banhart, Nanoscale order in the frustrated mixed conductor La5.6WO12-[delta], J. Appl. Cryst. 49 (3) (2016) 997–1008, https://doi.org/10.1107/S1600576716006415.

[20] A. Magraso, J.M. Polfus, C. Frontera, J. Canales-Vázquez, L.-E. Kalland, C. H. Hervoches, R. Haugsrud, Complete structural model for lanthanum tungstate: a chemically stable high temperature proton conductor by means of intrinsic defects, J. Mater. Chem. 22 (5) (2012) 1762–1764, https://doi.org/10.1039/C2JM14981H.

[21] K. Hack, T. Jantzen, M. Müller, E. Yazhenskikh, G. Wu, A novel thermodynamic database for slag systems and refractory materials, ICS 2012, Proceedings of the 5th International Congress on the Science and Technology of Steelmaking, Dresden, Germany, 2012.

[22] Database GTOx, GTT-Technologies, Forschungszentrum Jülich, 2010-2023, GTT-Technologies ⟨https://gtt-technologies.de/data/⟩.

[23] E. Yazhenskikh, K. Hack, M. Müller, Critical thermodynamic evaluation of oxide systems relevant to fuel ashes and slags, part 5: potassium oxide-alumina-silica, Calphad 35 (2011) 6–19, https://doi.org/10.1016/j.calphad.2010.10.010.

[24] T. Jantzen, E. Yazhenskikh, K. Hack, M. Müller, Thermodynamic assessment of the CaO–P_2O_5–SiO_2–ZnO system with special emphasis on the addition of ZnO to the Ca_2SiO_4–$Ca_3P_2O_8$ phase, Calphad 67 (2019) 101668, https://doi.org/10.1016/j.calphad.2019.101668.

[25] T. Jantzen, K. Hack, E. Yazhenskikh, M. Müller, Evaluation of thermodynamic data and phase equilibria in the system Ca-Cr-Cu-Fe-Mg-Mn-S part II: ternary and quasi-ternary subsystems, Calphad 56 (2017) 286–302, https://doi.org/10.1016/j.calphad.2017.01.007.

[26] E. Yazhenskikh, T. Jantzen, K. Hack, M. Müller, A new multipurpose thermodynamic database for oxide systems, Raplavy/Melts 2 (2) (2019) 116–124, https://doi.org/10.1134/S0235010619010237.

[27] H. Lukas, S.G. Fries, B. Sundman, Computational thermodynamics: the calphad method, Cambridge University Press, 2007.

[28] G.I. Tyushevskaya, N.S. Afonskii, V.I. Spitsyn, Study on phase composition in the system La_2O_3-WO_3, Dokl. Akad. Nauk (Russ.) 170 (4) (1966) 859–860.

[29] E.Y. Rode, G.M. Balagina, M.M. Ivanova, V.N. Karpov, Systems based on tungstates of rare-earth elements with tungstates of sodium and strontium, Zh. Neorg. Khim 13 (5) (1968) 1451–1456.

[30] M.M. Ivanova, G.M. Balagina, E.Y. Rode, Phase diagram of the system La_2O_3-WO_3, izw. Akad. nauk SSSR, Neorg. Mater. 6 (5) (1970) 914–919.

[31] M. Yoshimura, A. Rouanet, High temperature phase relations in the system La_2O_3-WO_3, Mat. Res. Bull. 11 (1976) 151–158.

[32] V.K. Yanovskii, V.I. Voronkova, Refinement of phase equilibria in the La_2O_3-WO_3 system, Inorg. Mater. (Engl. Transl.) 19 (3) (1983) 375–379.

[33] T.M. Besmann, K.E. Spear, Thermodynamic modelling of oxide glasses, J. Am. Ceram. Soc. 85 (12) (2002) 2887–2894, https://doi.org/10.1111/j.1151-2916.2002.tb00552.x.

[34] F.G. Casteels, M.J. Brabers, R. DePaus, Thermodynamic stability and phase equilibria in the system La-Th-W-O, Rev. Int. Hautes Temp. Refract 16 (1980) 424–436.

[35] M. Yoshimura, F. Sibieude, A. Rouanet, M. Foex, Polymorphism of R_2O_3•WO_3 (R=rare earth) compounds at high temperatures, Rev. Int. Hautes Temp. Refract 12 (3) (1975) 215–219.

[36] M. Yoshimura, A. Rouanet, F. Sibieude, Characterization and high-temperature phase relations of $3La_2O_3$•WO_3 and $5La_2O_3$•$2WO_3$, High. Temp. High. Press. 7 (1975) 227–234.

[37] C. Grenthe, M. Sundberg, V.P. Filonenko, I.P. Zibrov, High-Pressure tungsten bronzes, RE_xWO_3 with RE=La and nd, studied by X-Ray diffraction and electron microscopy, J. Solid State Chem. 154 (2) (2000) 466–475, https://doi.org/10.1006/jssc.2000.8866.

[38] V.P. Filonenko, C. Grenthe, M. Nygren, M. Sundberg, I.P. Zibrov, Structure and thermal stability of $La_{0.10}WO_{3+y}$; a hexagonal tungsten bronze related phase formed at high pressure, J. Solid State Chem. 163 (1) (2002) 84–92, https://doi.org/10.1006/jssc.2001.9376.

[39] T.I. Timchenko, L.V. Petushkova, E.A. Pobedimskaya, A.V. Pashkova, Lanthanum oxytungstate $2La_2O_3.3WO_3$, Dokl. Akad. Nauk SSSR 185 (3) (1969) 575–576.

[40] M. Yoshimura, H. Morikawa, M. Miyake, Preparation and cell parameters of new rare-earth tungstates $R_{10}W_{22}O_{81}$ (R = La, Ce, Pr and Nd), Mat. Res. Bull. 10 (11) (1975) 1221–1224, https://doi.org/10.1016/0025-5408(75)90030-6.

[41] K. Nassau, H.J. Levinstein, G.M. Loiacono, A comprehensive study of trivalent tungstates and molybdates of the type $L_2(MO_4)_3$, J. Phys. Chem. Solids 26 (12) (1965) 1805–1816, https://doi.org/10.1016/0022-3697(65)90213-1.

[42] M. Gärtner, D. Abeln, A. Pring, M. Wilde, A. Reller, Synthesis, structure, and reactivity of novel lanthanum tungstates, J. Solid State Chem. 111 (1) (1994) 128–133, https://doi.org/10.1006/jssc.1994.1207.

[43] Y. Laligant, A. Le Bail, F. Goutenoire, Ab initio structure determination of lanthanum Cyclo-tetratungstate α-$La_2W_2O_9$ from X-ray and neutron powder diffraction, J. Solid State Chem. 159 (1) (2001) 223–227, https://doi.org/10.1006/jssc.2001.9189.

[44] M.-H. Chambrier, A. Le Bail, S. Kodjikian, E. Suard, F. Goutenoire, Structure determination of $La_{18}W_{10}O_{57}$, Inorg. Chem. 48 (14) (2009) 6566–6572, https://doi.org/10.1021/ic9005482.

[45] M.H. Chambrier, S. Kodjikian, R.M. Ibberson, F. Goutenoire, Ab-initio structure determination of β-La_2WO_6, J. Solid State Chem. 182 (2) (2009) 209–214, https://doi.org/10.1016/j.jssc.2008.09.010.

[46] M.E. Ivanova, J. Seeger, J.M. Serra, C. Solis, W.A. Meulenberg, W. Fischer, H. P. Buchkremer, Influence of the $La_6W_2O_{15}$ phase on the properties and integrity of $La_{6-x}WO_{12-\delta}$–Based membranes, chem. Mater, Research 2 (1) (2012) 56–82.

[47] M.H. Chambrier, R.M. Ibberson, F. Goutenoire, Structure determination of α-$La_6W_2O_{15}$, J. Solid State Chem. 183 (6) (2010) 1297–1302, https://doi.org/10.1016/j.jssc.2010.03.043.

[48] M.-H. Chambrier, A. Le Bail, F. Giovannelli, A. Redjaïmia, P. Florian, D. Massiot, F. Goutenoire, $La_{10}W_2O_{21}$: an anion-deficient fluorite-related superstructure with oxide ion conduction, Inorg. Chem. 53 (1) (2014) 147–159, https://doi.org/10.1021/ic401801u.

[49] L.L.Y. Chang, B. Phillips, Samarium and lanthanum tungstates of the $3R_2O_3.WO_3$ type, Inorg. Chem. 3 (12) (1964) 1792–1794, https://doi.org/10.1021/ic50022a036.

[50] A.A. Nadiradze, L.D. Chanturishvili, G.G. Gwelesiani, Enthalpy and heat capacity of tungsten oxides of lanthanum at high temperatures, inst. Metallurgy, Akad. Sci. Georgian SSR 17 (3) (1979) 436–439.

[51] L.D. Chanturishvili, A.A. Nadiradze, G.G. Gwelesiani, Study on high temperature enthalpy and heat capacity $La_{14}W_8O_{45}$, $La_2W_2O_9$, $La_2(WO_4)_3$ and $La_{10}W_{22}O_{81}$, Bull. Acad. Sci. Georgian SSR 94 (1) (1979) 97–100.

[52] V.N. Chentsov, Y.Y. Skolis, V.A. Levitskii, Thermodynamic properties of $3La_2O_3$•WO_3 at high temperatures, Neorg. Mater. 9 (9) (1973) 1591–1595.

[53] V.A. Levitskii, V.N. Chentsov, Y.Y. Skolis, A.N. Klimenko, V.P. Marin, Y. V. Men`shenin, Thermodynamic of interaction of some refractory oxides type R_2O_3 with tungsten and its oxide, Neorg. Mater. 16 (6) (1980) 949–958.

[54] V.A. Levitskii, V.N. Chentsov, Y.Y. Skolis, J.I. Gerassimov, Thermodynamics of refractory double oxide. Interaction of Y_2O_3, La_2O_3, Dy_2O_3, Nd_2O_3 and Al_2O_3 with tungsten and its oxidation products, Rev. Int. Hautes Temp. Refract 17 (1980) 82–98.

[55] L.D. Chanturishvili, A.A. Nadiradze, G.G. Gwelesiani, Study of thermodynamic properties of lanthanum oxitungsates izw. Akad. nauk Georgian SSR, Chemistry 4 (2) (1978) 135–140.

[56] L.D. Chanturishvili, A.A. Nadiradze, G.G. Gwelesiani, Measurement of the free energy of lanthanum tungstates, Bull. Acad. Sci. Georgian SSR 92 (3) (1978) 645–648.

[57] S. Raghavan, Thermodynamic stabilities of lanthanum tungstates using a calcium fluoride solid electrolyte galvanic cell, Miner. Process. Extr. Metall. Rev. 22 (1) (2001) 221–230, https://doi.org/10.1080/08827509808962497.

[58] G.G. Gwelesiani, D.S. Zagarejshwili, A.A. Nadiradze, Thermodynamic of oxygen containing compounds of the rare-earth metals at high temperatures, Akad. Nauk Georgian SSR, Institut of metallurgy, Tbilisi: Meznierba, Tbilisi, 1983.

[59] A.A. Nadiradze, About calculation of standard entropy of the rare-earth tungstates, Bull. Acad. Sci. Georgian SSR 122 (1) (1986) 113–116.

[60] A.A. Nadiradze, Equation for calculation of the standard formation enthalpy of the rare-earth tungstates, izw. Akad. nauk Georgian SSR, Chemistry 13 (3) (1987) 185–189.

[61] A. Lashtabeg, J. Bradley, A. Dicks, G. Auchterlonie, J. Drennan, Structural and conductivity studies of $Y_{10-x}La_xW_2O_{21}$, J. Solid State Chem. 183 (5) (2010) 1095–1101, https://doi.org/10.1016/j.jssc.2010.03.009.

[62] A. Magraso, C. Frontera, D. Marrero-López, P. Nunez, New crystal structure and characterization of lanthanum tungstate "La_6WO_{12}" prepared by freeze-drying synthesis, Dalton Trans. (2009) 10273–10283, https://doi.org/10.1039/b916981b.

[63] A. Magraso, R. Haugsrud, Effects of the La/W ratio and doping on the structure, defect structure, stability and functional properties of proton-conducting lanthanum tungstate $La_{28-x}W_{4+x}O_{54+d}$. a review, J. Mater. Chem. A 2 (2014) 12630–12641, https://doi.org/10.1039/C4TA00546E.

[64] J. Seeger, M.E. Ivanova, W.A. Meulenberg, D. Sebold, D. Stöver, T. Scherb, J. M. Serra, Synthesis and characterization of nonsubstituted and substituted Proton-Conducting $La_{6-x}WO_{12-y}$, inorg, Chem 52 (18) (2013) 10375–10386, https://doi.org/10.1021/ic401104m.

[65] A. Fantin, T. Scherb, J. Seeger, G. Schumacher, U. Gerhards, M.E. Ivanova, J. Banhart, Relation between composition and vacant oxygen sites in the mixed ionic-electronic conductors $La_{5.4}W_{1-y}M_yO_{12-\delta}$ (M=Mo, Re; $0 \leq y \leq 0.2$) and their mother compound $La_{6-x}WO_{12-\delta}$ ($0.4 \leq x \leq 0.8$), Solid State Ion. 306 (2017) 104–111, https://doi.org/10.1016/j.ssi.2017.04.005.

[66] A. Fantin, T. Scherb, J. Seeger, G. Schumacher, U. Gerhards, M.E. Ivanova, J. Banhart, Crystal structure of Mo-substituted lanthanum tungstate $La_{5.4}W_{1-y}Mo_yO_{12-[delta]}$ ($0 <= y <= 0.2$) studied by X-ray and neutron diffraction, J. Appl. Cryst. 52 (5) (2019) 1043–1053, https://doi.org/10.1107/S1600576719009385.

[67] S. Erdal, L.-E. Kalland, R. Hancke, J. Polfus, R. Haugsrud, T. Norby, A. Magrasó, Defect structure and its nomenclature for mixed conducting lanthanum tungstates $La_{28-x}W_{4+x}O_{54+3x/2}$, Int. J. Hydrog. Energy 37 (9) (2012) 8051–8055, https://doi.org/10.1016/j.ijhydene.2011.11.093.

[68] H. Ehrenberg, T. Hartmann, K.G. Bramnik, G. Miehe, H. Fuess, Yttrium rhenium oxide, $Y_7ReO_{14-\delta}$: a cubic fluorite superstructure, Solid State Sci. 6 (3) (2004) 247–250, https://doi.org/10.1016/j.solidstatesciences.2004.02.003.

[69] *SGPS - SGTE Pure Substances database* (*v13.1*) 2019,

[70] M.W. Chase, Jr, NIST-JANAF thermochemical tables, fourth edition, parts I and II, j, Phys. Chem. Ref. Data Monogr. 9 (1998) 1963.

[71] A.N. Grundy, B. Hallstedt, L.J. Gauckler, Thermodynamic assessment of the lanthanum-oxygen system, J. Phase Equilib. 22 (2) (2001) 105–113, https://doi.org/10.1361/105497101770338950.

[72] SGTE 2022 intermetallic compounds, 2022, SGTE Scientific Group Thermodata Europe.

[73] M. Hillert, The compound energy formalism, J. Alloys Compd. 320 (2001) 161-176.

[74] *FactSage: Facility for the Analysis of Chemichal Thermodynamics, Version 8.3*. ⟨www.factsage.com/⟩ 1976-2024; Available from: ⟨http://www.factsage.com/⟩.

[75] B. Reis, F. Tang, P. Keuter, Mt Baben, User-friendly and robust calphad optimizations using calphad optimizer in FactSage, Calphad 88 (2025) 102800, https://doi.org/10.1016/j.calphad.2025.102800.

[76] H.A. Wriedt, The O−W (Oxygen-Tungsten) system, Bull. Alloy Phase Diagr. 10 (4) (1989) 368–384.

[77] D.H. Dennison, M.J. Tschetter, K.A. Gschneidner, The solubility of tantalum and tungsten in liquid rare-earth metals, J. LessCommon Met 11 (6) (1966) 423–435, https://doi.org/10.1016/0022-5088(66)90089-0.

[78] F. Gaume-Mahn, C. Ait-Yahia, Etude de l'attaque du rhenium et du tungstene purs par le lanthane et le cerium fondus, C. R. Acad. Sc. C. 262 (1966) 1528–1529.

[79] B. Predel, La-W (Lanthanum-Tungsten): Datasheet from Landolt-Börnstein - Group IV Physical Chemistry · Volume 5G: "Hg-Ho – La-Zr" in SpringerMaterials (https://doi.org/10.1007/10506626_1900), O. Madelung, Editor. 1997, Springer-Verlag Berlin Heidelberg.

[80] H. Okamoto, La-W (lanthanum-tungsten), J. Phase Equilib. 22 (6) (2001) 693, https://doi.org/10.1007/s11669-001-0048-4.

[81] N. Krishnamurthy, T. Kundu, A. Awasthi, S.P. Garg, Derived thermodynamic properties and phase diagrams of the rare Earth-Tungsten systems, Z. Met. 91 (3) (2000) 234–240.

[82] M. Yoshimura, T. Sata, T. Nakamura, Nippon kagaku kaishi, J. Chem. Soc. Jpn.) (1974) 2287.

[83] V.E. Plyuschev, V.M. Amosov, Synthesis and properties of the tungstates of la, ce, pr and nd, Neorg. Mater. 1 (7) (1965) 1155–1161.

[84] L.H. Brixner, A.W. Sleight, Crystal growth and precision lattice constants of some $Ln_2(WO_4)_3$-type rare earth tungstates, Mater. Res. Bull. 8 (10) (1973) 1269–1273, https://doi.org/10.1016/0025-5408(73)90165-7.

[85] K. Nassau, J.W. Shiever, E.T. Keve, Structural and phase relationships among trivalent tungstates and molybdates, J. Solid State Chem. 3 (1971) 411–419.

[86] V.E. Plyuschev, V.M. Amosov, Thermochemical characteristics of the middle tungstates of la and lanthanides, Zh. Neorg. Khim 13 (9) (1968) 2421–2427.

[87] Ab initio materials project (AIMP) compound database using data from ⟨www.materialsproject.org⟩ *as input.*, GTT-Technologies, 2022,

[88] V.P. Glushko, Termicheskie Kostanty (Thermal Constants of Substances), in Online reference book: www.chem.msu.ru/cgi-bin/tkv.pl?show=welcome.html. 1965-1982, Moscow State University, Chemical Department: Moscow.

[89] V.E. Plyuschev, V.M. Amosov, Thermochemical characteristic of middle tungstates of elements belonging to the sub-group of sc and lanthanides, Izv. Viss. Uchebn. Zaved. Zvet. Met. 89 (3) (1970) 89–94.

[90] V.N. Chentsov, Thermodynmaic study of some catode materials based on the rare earth oxides and aluminium. Chemistry Department, Moscow State University: Moscow, 1974.

[91] J.A. Collado, M.A.G. Aranda, A. Cabeza, P. Olivera-Pastor, S. Bruque, Synthesis, structures, and thermal expansion of the $La_2W_{2-x}Mo_xO_9$ series, J. Solid State Chem. 167 (1) (2002) 80–85, https://doi.org/10.1006/jssc.2002.9622.

[92] D. Marrero-López, J. Peña-Martínez, J.C. Ruiz-Morales, P. Núñez, Phase stability and ionic conductivity in substituted $La_2W_2O_9$, J. Solid State Chem. 181 (2) (2008) 253–262, https://doi.org/10.1016/j.jssc.2007.11.024.

[93] N.E. Novikova, T.A. Sorokin, A.M. Antipin, N.B. Bolotina, O.A. Alekseeva, N. I. Sorokina, V.I. Voronkova, Characteristic features of polytypism in compounds with the $La_{18}W_{10}O_{57}$-type structure, Acta Cryst. C. 75 (6) (2019) 740–749, https://doi.org/10.1107/S2053229619006107.

[94] M.-H. Chambrier, F. Goutenoire, Structural exploration on powder diffraction a nice tool for rexamination of phase diagram, JEEP 00022 (2009), https://doi.org/10.1051/JEEP%2F200900022.

[95] M. Allix, M.-H. Chambrier, E. Véron, F. Porcher, M. Suchomel, F. Goutenoire, Synthesis and structure determination of the high temperature form of La_2WO_6, Cryst. Growth Des. 11 (11) (2011) 5105–5112, https://doi.org/10.1021/cg201010y.

[96] G.G. Gwelesiani, I.B. Baratashwili, I.S. Omiadze, A.A. Nadiradze, High temperature enthalpy and heat capacity of Nd_2WO_6, Eu_2WO_6, Er_2WO_6 and $Eu_2(WO_4)_3$, Izv. Akad. Nauk Georgian SSR 14 (2) (1988) 117–125.

[97] M. Foex, Une famille de composes refractaires: le tungstates du type R_6WO_{12}, Bull. Soc. Chim. Fr. 10 (1967) 3696.

[98] V.A. Levitski, V.N. Chentsov, Y.Y. Skolis, Thermodynamic of binary oxide systems at high temperatures. Part VII: interaction of Y_2O_3 and La_2O_3 with w in vacuum, Zh. Fiz. Khim 48 (3) (1974) 566–569.

[99] M. Yoshimura, J. Coutures, M. Foex, Rapid quenching of melts in the system La_2O_3-WO_3, J. Mater. Sci. 12 (2) (1977) 415–417, https://doi.org/10.1007/BF00566286.

[100] G. Kojo, Y. Shono, H. Ushiyama, Y. Oshima, J. Otomo, Influence of La/W ratio on electrical conductivity of lanthanum tungstate with high La/W ratio, J. Solid State Chem. 248 (2017) 1–8, https://doi.org/10.1016/j.jssc.2017.01.011.

[101] M. Heyrman, C. Chatillon, A. Pisch, Congruent vaporization properties as a tool for critical assessment of thermodynamic data: the case of gaseous molecules in the La–O and Y–O systems, Calphad 28 (1) (2004) 49–63, https://doi.org/10.1016/j.calphad.2004.03.001.

[102] C. Younes, Contribution a l`etude thermodynamique par spectrometrie de masse a haute temperature des oxydes MO2-x (M=U, (U, La), (La, Ce), (La, Ce, Y), (U, Ce)), Universite de Paris-Sud: Paris, 1986.

[103] R.J. Ackermann, E.G. Rauh, A high temperature study of the stoichiometry, phase behavior, vaportization characteristics, and thermodynamic properties of the lanthanum+oxygen system, J. Chem. Thermodyn. 3 (4) (1971) 445–460, https://doi.org/10.1016/S0021-9614(71)80027-7.

[104] P.N. Walch, H.W. Goldstein, D. White, Vaporisation of rare-earth oxides, J. Am. Ceram. Soc. 43 (5) (1960) 229–233.